



HAL
open science

Investigation of the homogeneity of energy conversion processes at dipolarization fronts from MMS measurements

S. W. Alqeeq, O. Le Contel, Patrick Canu, Alessandro Retinò, Thomas Chust, Laurent Mirioni, L. Richard, Y. Aït-Si-Ahmed, A. Alexandrova, A. Chuvatin, et al.

► To cite this version:

S. W. Alqeeq, O. Le Contel, Patrick Canu, Alessandro Retinò, Thomas Chust, et al.. Investigation of the homogeneity of energy conversion processes at dipolarization fronts from MMS measurements. *Physics of Plasmas*, 2022, 29 (1), pp.012906. 10.1063/5.0069432 . hal-03573187

HAL Id: hal-03573187


<https://hal.sorbonne-universite.fr/hal-03573187>

Submitted on 14 Feb 2022

HAL is a multi-disciplinary open access archive for the deposit and dissemination of scientific research documents, whether they are published or not. The documents may come from teaching and research institutions in France or abroad, or from public or private research centers.

L'archive ouverte pluridisciplinaire **HAL**, est destinée au dépôt et à la diffusion de documents scientifiques de niveau recherche, publiés ou non, émanant des établissements d'enseignement et de recherche français ou étrangers, des laboratoires publics ou privés.

AUTHOR QUERY FORM

	<p>Journal: Phys. Plasmas</p> <p>Article Number: POP21-AR-MMS2021-01348</p>	<p>Please provide your responses and any corrections by annotating this PDF and uploading it to AIP's eProof website as detailed in the Welcome email.</p>
---	---	--

Dear Author,

Below are the queries associated with your article; please answer all of these queries before sending the proof back to AIP.

Article checklist: In order to ensure greater accuracy, please check the following and make all necessary corrections before returning your proof.

1. Is the title of your article accurate and spelled correctly?
2. Please check affiliations including spelling, completeness, and correct linking to authors.
3. Did you remember to include acknowledgment of funding, if required, and is it accurate?

Location in article	Query / Remark: click on the Q link to navigate to the appropriate spot in the proof. There, insert your comments as a PDF annotation.
AQ1	Please check that the author names are in the proper order and spelled correctly. Also, please ensure that each author's given and surnames have been correctly identified (given names are highlighted in red and surnames appear in blue).
AQ2	Please define LHDI at first occurrence.
AQ3	Please specify which sections "in the next sections" refer to in the sentence beginning "They are mentioned as they ..."
AQ4	In sentence beginning "One can see that electrons ...," please confirm that "the next section" refers to Sec. VI.
AQ5	In sentence beginning "Conversely, the current density remains..." please confirm that "next section" refers to Sec. VII.
AQ6	Refs. 58 and 59 were not cited in your original manuscript. We have inserted a citation for them in the sentence beginning "This latter contribution can be..." Please carefully review our placement of the citation and confirm that it is correct. If it is not correct, mark the citation for deletion and specify where the citation for Refs. 58 and 59 should be inserted.
AQ7	Please provide publisher name for Ref. 44.
AQ8	We were unable to locate a digital object identifier (doi) for Ref(s). 5, 8, 10, 18, 29, 45, and 48. Please verify and correct author names and journal details (journal title, volume number, page number, and year) as needed and provide the doi. If a doi is not available, no other information is needed from you. For additional information on doi's, please select this link: http://www.doi.org/ .
AQ9	Please provide journal title for Ref. 55.
	Please confirm ORCID's are accurate. If you wish to add an ORCID for any author that does not have one, you may do so now. For more information on ORCID, see https://orcid.org/ .
	S. W. Alqeeq - 0000-0002-5401-6644
	O. Le Contel - 0000-0003-2713-7966

P. Canu-
A. Retinò-
T. Chust-
L. Mirioni-
L. Richard-
Y. Aït-Si-Ahmed-
A. Alexandrova-
A. Chuvatin-
N. Ahmadi - 0000-0001-5267-0485
S. M. Baraka - 0000-0001-6748-6795
R. Nakamura - 0000-0002-2620-9211
F. D. Wilder-
D. J. Gershman - 0000-0003-1304-4769
P. A. Lindqvist - 0000-0001-5617-9765
Yu. V. Khotyaintsev - 0000-0001-5550-3113
R. E. Ergun-
J. L. Burch - 0000-0003-0452-8403
R. B. Torbert-
C. T. Russell-
W. Magnes-
R. J. Strangeway-
K. R. Bromund-
Hanying Wei-
F. Plaschke-
B. J. Anderson-
B. L. Giles-
S. A. Fuselier-
Y. Saito-
B. Lavraud-

Please check and confirm the Funder(s) and Grant Reference Number(s) provided with your submission:

Centre National d'Etudes Spatiales, Award/Contract Number

Institut des sciences de l'ingénierie et des systèmes, Award/Contract Number

Please add any additional funding sources not stated above:

Thank you for your assistance.

Dear Author,

While reviewing your paper, we have identified additional changes that were necessary and have noted them on the proof. Please retain our changes and write "approve" or "reject" next

Investigation of the homogeneity of energy conversion processes at dipolarization fronts from MMS measurements

Cite as: Phys. Plasmas **29**, 000000 (2022); doi: 10.1063/5.0069432

Submitted: 31 August 2021 · Accepted: 15 December 2021 ·

Published Online: 0 Month 0000



AQ1

S. W. Alqeeq,^{1,a)} O. Le Contel,¹ P. Canu,¹ A. Retinò,¹ T. Chust,¹ L. Mirioni,¹ L. Richard,^{2,3} Y. Aït-Si-Ahmed,¹ A. Alexandrova,¹ A. Chuvatin,¹ N. Ahmadi,⁴ S. M. Baraka,⁵ R. Nakamura,⁶ F. D. Wilder,⁷ D. J. Gershman,⁸ P. A. Lindqvist,⁹ Yu. V. Khotyaintsev,² R. E. Ergun,⁴ J. L. Burch,¹⁰ R. B. Torbert,¹¹ C. T. Russell,¹² W. Magnes,⁶ R. J. Strangeway,¹² K. R. Bromund,⁸ Hanying Wei,¹² F. Plaschke,⁶ B. J. Anderson,¹³ B. L. Giles,⁸ S. A. Fuselier,¹⁰ Y. Saito,¹⁴ and B. Lavraud¹⁵

AFFILIATIONS

¹Laboratoire de Physique des Plasmas (LPP), UMR7648, CNRS, Sorbonne Université, Université Paris-Saclay, Observatoire de Paris, Ecole Polytechnique Institut Polytechnique de Paris, Paris 75005, France.

²Swedish Institute of Space Physics, Uppsala 75236, Sweden

³Department of Physics and Astronomy, Uppsala University, Uppsala 75236, Sweden

⁴Laboratory for Atmospheric and Space Physics, University of Colorado, Boulder, Colorado 80303, USA

⁵National Institute of Aerospace, Hampton University, Hampton, Virginia 23666, USA

⁶Space Research Institute, Austrian Academy of Sciences, Graz 8042, Austria

⁷Physics Faculty, University of Texas, Arlington, Texas 76019, USA

⁸NASA Goddard Space Flight Center, Greenbelt, Maryland 20771, USA

⁹Royal Institute of Technology, Stockholm 11428, Sweden

¹⁰Southwest Research Institute, San Antonio, Texas 78238, USA

¹¹Space Science Center and Department of Physics, University of New Hampshire, Durham, New Hampshire 03824, USA

¹²Department of Earth, Planetary and Space Sciences, University of California, Los Angeles, California 90095, USA

¹³Applied Physics Laboratory, The Johns Hopkins University, Laurel, Maryland 20723, USA

¹⁴Institute for Space and Astronautical Science, Sagami-hara, Kanagawa 252-5210, Japan

¹⁵Institut de Recherche en Astrophysique et Planétologie (IRAP), CNRS UMR5277/Université Paul Sabatier, Toulouse 31400, France

Note: This paper is a part of the Special Collection: Plasma Physics from the Magnetospheric Multiscale Mission.

a) Author to whom correspondence should be addressed: alqeeq@lpp.polytechnique.fr

ABSTRACT

We report on six dipolarization fronts (DFs) embedded in fast earthward flows detected by the Magnetospheric Multiscale mission during a substorm event on 23 July 2017. We analyzed the Ohm's law for each event and found that ions are mostly decoupled from the magnetic field by the Hall fields. However, the electron pressure gradient term is also contributing to the ion decoupling and likely responsible for an electron decoupling at DF. We also analyzed the energy conversion process and found that the energy in the spacecraft frame is transferred from the electromagnetic field to the plasma ($\mathbf{J} \cdot \mathbf{E} > 0$) ahead or at the DF, whereas it is the opposite ($\mathbf{J} \cdot \mathbf{E} < 0$) behind the front. This reversal is mainly due to a local reversal of the cross-tail current indicating a substructure of the DF. In the fluid frame, we found that the energy is mostly transferred from the plasma to the electromagnetic field ($\mathbf{J} \cdot \mathbf{E}' < 0$) and should contribute to the deceleration of the fast flow. However, we show that the energy conversion process is not homogeneous at the electron scales due to electric field fluctuations likely related to lower-hybrid drift waves. Our results suggest that the role of DF in the global energy cycle of the magnetosphere still deserves more investigation. In particular, statistical studies on DF require to be carried out with caution due to these electron scale substructures.

Published under an exclusive license by AIP Publishing. <https://doi.org/10.1063/5.0069432>

45 I. INTRODUCTION

46 Fast plasma flows in the magnetotail have been investigated for a
47 long time thanks to *in situ* space measurements. They contribute sig-
48 nificantly to the energy, plasma, and magnetic flux transports in the
49 Earth's magnetosphere.^{1–4} They are thought to be generated by mag-
50 netic reconnection,^{5–7} kinetic ballooning interchange instability,⁸ or
51 low entropy magnetic flux tubes;⁹ they can be related to a global scale
52 substorm activity or appear as isolated structures. Dipolarization fronts
53 (DFs), which are mostly characterized by a sharp and transient
54 increase in the normal component (northward) of the magnetic field
55 in the magnetotail, are formed by the plasma flow propagation or can
56 be also embedded in the flow. The sharp increase in the magnetic field
57 is often interpreted as the magnetic field pile up behind the front.
58 These fronts can be also preceded by a decrease in the normal compo-
59 nent.^{10–12} The whole spatial scale of DF is about few ion inertial
60 lengths (c/ω_{pi} , where ω_{pi} is the ion plasma frequency).^{13–15} A recent
61 review by Fu *et al.* has focused on their important role in particle accel-
62 eration mechanisms.¹⁶

63 Angelopoulos *et al.* suggested that the DF could play an impor-
64 tant role in the energy conversion process due to their large scale prop-
65 agation through the Earth's magnetosphere.¹⁷ Based on data from the
66 THEMIS mission, they showed that energy conversion occurs within
67 an electron scale current sheet (1–10 electron inertial lengths) gener-
68 ated by DF propagation. Integrated all along the propagation mostly
69 along the X geocentric solar magnetospheric (GSM) direction and
70 assuming a transverse Y–Z section of about $10 R_E^2$, the authors sug-
71 gested that DFs are able to provide a macroscopic energy conver-
72 sion. Therefore, the estimate of the energy conversion at DFs seems
73 to be crucial to understand the global energy cycle in the Earth's
74 magnetosphere.

75 This question is also fundamental for the fast flow propagation
76 itself. Indeed, as the fast flow propagates, the fraction of energy that it
77 can lose due to various energy conversion processes contributes to its
78 braking. Using THEMIS data, Chaston *et al.*¹⁸ suggested that kinetic
79 Alfvén waves continually radiated toward the auroral region by fast
80 flows during their earthward propagation can extract the total kinetic
81 energy from the flows. Later Hamrin *et al.*¹⁹ found indications of fast
82 flow decelerations in the range $-25 < X < -15 R_E$ and investigated
83 the related energy conversion processes by computing the $\mathbf{J} \cdot \mathbf{E}$ term
84 where (\mathbf{J} is the current density and \mathbf{E} the electric field in the spacecraft
85 frame). Thanks to a superposed epoch analysis applied on Cluster
86 data, they found that fast flows with a velocity peak behind the front
87 are decelerated and that energy is radiated, i.e., converted from par-
88 ticles to fields, whereas, when the velocity peak is detected ahead or at
89 DF, no braking signature is detected and energy is transferred from
90 fields to particles (dissipation). Still from statistical analysis of 2003
91 Cluster data corresponding to an average subproton scale spacecraft
92 separation of 200 km, Huang *et al.*²⁰ found that the energy was signifi-
93 cantly transferred from the fields to the plasma at DFs. More recently,
94 using data gathered during the Magnetospheric Multiscale (MMS)
95 commissioning phase and with a better time resolution for particle
96 measurements (150 ms for ions, 30 ms for electrons), Yao *et al.*²¹
97 showed that electron contribution to the DF current density is signifi-
98 cant (60% of ions) and produced by the diamagnetic effect. With
99 regard to the energy conversion, they found that the field energy is
100 transferred to the plasma in the spacecraft frame though the velocity
101 peak is detected behind the DF. In the fluid frame (ion or electron),

they pointed out that the energy transfer is from particles to fields. 102
Later Liu *et al.*²² showed that ion scale DFs can be also associated with 103
electron scale current sheets. They specify that although their DF event 104
corresponded primarily to an energy transfer from fields to particles, 105
the electron scale currents could also lead to radiating the plasma 106
energy. Such electron scale DF substructures were also reported in 107
previous studies and attributed to the lower-hybrid drift instability grow- 108
ing in the density gradient region^{23–26} leading to ripples on the DF.²⁷ 109
Later, these results were confirmed by a statistical study carried out by 110
Zhong *et al.*²⁸ based on 122 DF events detected by MMS in the magne- 111
totail. The contribution of broad band high-frequency waves (with 112
frequencies between the electron gyrofrequency and the plasma fre- 113
quency) was also investigated and shown to be up to 10% of the total 114
energy conversion at DF.²⁶ Finally, Zhang *et al.*²⁹ suggested that both 115
Joule dissipation via parallel and perpendicular currents and radiated 116
energy by kinetic Alfvén waves contribute to the fast flow slowdown. 117

Energy conversion processes have also been investigated recently 118
by 3D kinetic particle-in-cell (PIC) simulations. The role of the lower- 119
hybrid drift instability rising at DFs was also investigated and pointed 120
out as a significant element of the DF dynamics.³⁰ Later, comparing 121
3D PIC simulation results and Cluster observations Khotyaintsev *et al.* 122
concluded that the energy dissipation in the satellite (Earth) frame was 123
mainly due to the motional electric field and the ion contribution to 124
the current, suggesting that LHDI was not contributing to the energy 125
conversion process. They found almost no energy conversion in the 126
DF frame (defined by using the ion velocity at the DF).³¹ Using recent 127
theoretical developments in turbulence studies by Yang *et al.*,³² which 128
allow to disentangle ion and electron contributions, Sitnov *et al.*³³ 129
showed that ions are heated at and ahead of DFs, whereas electrons 130
are heated at and behind due to the long-wavelength lower-hybrid 131
drift instability; therefore, both contributions lead to an important 132
energy dissipation. Finally, Nakamura *et al.*³⁴ also carried out 3D PIC 133
simulations and reported that energy is dissipated in the electron 134
frame at DFs within the density gradient layer due to the lower-hybrid 135
instability. Their numerical results were shown to be in good agree- 136
ment with the recent MMS observations described by Liu *et al.* 137
although the energy conversion term was estimated in the electron 138
frame for the simulations and in the satellite frame for the 139
observations.²² 140

In the present study, we investigate the energy conversion processes 141
for six DFs embedded in fast earthward flows detected by MMS 142
on 23 July 2017. Data and methods are described in Sec. II. An over- 143
view of basic DF properties is presented in Sec. III. In Sec. IV, we pre- 144
sent a cross-validation of current density calculations and of Hall 145
electric fields. Ion and electron dynamics are investigated thanks to the 146
Ohm's law in Sec. V; then, the energy conversion processes at the 147
vicinity of these six DFs are scrutinized in Sec. VI. Finally, we summa- 148
rize and discuss the global results of this study in Sec. VII. 149

150 II. DATA AND METHODS

151 A. Data

In the present study, we analyze the various physical quantities 152
measured by the MMS instrument suite.^{35,36} DF properties are charac- 153
terized thanks to the magnetic field measurements provided by the 154
fluxgate magnetometer (FGM) with a sampling frequency of 128 Hz 155
in burst mode,³⁷ the electric field measurements (EDP) sampled at 156
32 Hz in fast survey mode,^{38,39} the ion and electron moment 157

AQ2

158 measurements provided by the fast plasma investigation suite (FPI)
159 sampled at 150 and 30 ms, respectively.⁴⁰ However, due to the very
160 low density in the magnetotail ($<0.05 \text{ part}\cdot\text{cm}^{-3}$), we have used the
161 electron partial moments provided by the FPI team for which the inte-
162 gration of the distribution function starts at the minimum energy of
163 100 eV. Furthermore, in order to reduce even more the noise on elec-
164 tron moments, we have time averaged the electron data at 0.3 s.
165 Hence, all results shown in this study are based on data with a 0.3 s
166 time resolution. Background noise produced by energetic electrons
167 penetrating the ion detectors has been subtracted from ion FPI mea-
168 surements as recommended by the FPI team.⁴¹ The upper energy limit
169 of FPI is 30 keV; therefore, ion moment calculations can be still inac-
170 curate in the magnetotail where ions can be more energetic, as we will
171 see by comparing them with the particle measurements from the hot
172 plasma composition analyzer (HPCA), which has a higher energy cut-
173 off and a time resolution of 10 s.⁴²

174 Throughout the paper, current densities from FPI measurements
175 ($\mathbf{J}_{part} = en_e(\mathbf{v}_i - \mathbf{v}_e)$) are computed using single spacecraft data,
176 which have been time averaged at 0.3 s. Also, we compute a four-
177 spacecraft average of these single satellite current densities in order to
178 compare with the current estimated from the curlometer technique⁴³
179 given by $\mathbf{J}_{curl} = (\nabla \times \mathbf{B})/\mu_0$. This comparison allows us to verify the
180 reliability of the particle moments despite the instrumental issues
181 mentioned above. The use of HPCA proton moments in the current
182 density calculations does not modify the results as the current is most
183 of the time dominated by the electron motion.

184 Finally, data used in the present study were gathered by MMS on
185 the 23 July 2017 when the constellation was located on the dusk side of
186 the magnetotail [$X = -23.9$, $Y = 5.8$, $Z = 5.4$] Earth radii (R_E) in the
187 geocentric solar ecliptic coordinate system (GSE). The average spacecraft
188 separation was about 15 km, i.e., close to the scale of the average electron
189 Larmor radius during this period (in average between 40 and 60 km).

190 Between 16:45 and 17:15 UT, MMS detected successive fast
191 earthward flows, which occurred during a substorm period as indi-
192 cated by the auroral electrojet—AE index $\sim 400 \text{ nT}$ (courtesy of Kyoto
193 World data Center for Geomagnetism: http://wdc.kugi.kyoto-u.ac.jp/ae_provisional/201707/index_20170723.html).

194 In Sec. III, six DF signatures embedded in these fast flows are
195 described.
196

197 B. Methods

198 DFs can be described locally (at the scale of a single satellite) as
199 1D tangential discontinuities.^{11,23} Therefore, DF signatures are usually
200 displayed in a local coordinate system obtained from a minimum vari-
201 ance analysis⁴⁴ applied on magnetic fields data (MVAB) of a single
202 spacecraft^{20,22} and/or from a timing analysis in case of a multi-
203 spacecraft missions.⁴⁵ MVAB is applied over the time period corre-
204 sponding to the sharp increase of northward component (B_z) of the
205 four spacecraft average of the magnetic field measurement. MVAB
206 applied on single spacecraft magnetic field data gives similar LMN
207 frames. Note that when additional structures ahead or behind the DF
208 are identified, they are excluded to the time period used for MVAB.

209 III. OVERVIEW OF CLASSICAL DF PROPERTIES

210 In this section, we describe the global properties of six DF events,
211 each one embedded in a fast earthward flow detected by MMS
212 between 16:45 and 17:15 UT.

Figure 1 shows these six DF events denoted DF1, DF2a,b, DF3a,b, and DF4 in their respective LMN frame obtained from the MVAB. For each event, the MVAB results are summarized in Table I, and the time period used is indicated. From these MVAB results, we define L , M , and N vectors as maximum, intermediate, and minimum variance directions, respectively. We have verified that the ratio between the three corresponding eigenvalues, $\lambda_1, \lambda_2, \lambda_3$, is sufficiently large (>10 in average though three ratios are between 2 and 10) to indicate that the three directions are well separated (see Table I). Table II shows the components of the normal estimated by a timing analysis as well as the velocity along the normal in GSE. The estimated thickness δ of each DF event is also given (in km and in d_p , the ion inertial length estimated based on the plasma sheet density prior to respective DF arrival) by multiplying the normal DF velocity by the time interval between the minimum and maximum of B_L .³¹ Note that in accordance with the propagation direction given by timing analysis, the orientation of the N vector of the MVAB was set to be positive (earthward) and L always oriented northward leading to M directed downward. Normal directions obtained from the two methods are qualitatively consistent and indicate that DFs are mainly oriented earthward (along X GSE), some DFs having a significant duskward component (along Y GSE) and southward component (along $-Z$ GSE). DF normal velocities range from 135 to 481 km/s. As the angle between the DF2a and DF2b normals (respectively, DF3a and DF3b) is $\sim 12.7^\circ$ (respectively, $\sim 22.2^\circ$), and for the sake of simplicity, only DF2a and DF3a LMN frames are used for plotting DF2 and DF3 periods. We checked that similar results are obtained when individual LMN frames are used. The estimated thickness of the DFs ranges from 0.98 to 3.78 d_p as found in previous THEMIS,¹¹ Cluster,^{14,46} and MMS^{15,21,22,31} studies.

Figure 1 displays ion scale properties of these six DFs. Magnetic field components and magnitude are plotted in Fig. 1(a), FPI ion velocity components and the N component of the HPCA velocity (V_{H+}) are shown in Fig. 1(b), ion and electron temperatures are shown in Fig. 1(c), electron density us shown in Fig. 1(d), and finally ion and electron pressure variations are shown in Fig. 1(e). These six DF events are identified by a vertical red dashed line (maximum of the B_L component). Vertical black dashed lines indicate possible signatures of flux ropes (large increase in the total magnetic field due to an increase in the cross-tail M component, associated with a bipolar signature of another component) ahead of these DF signatures. The detailed description of these flux ropes is beyond the scope of this study. They are mentioned as they can drive their own energy conversion processes as we will see in the next sections.

The six DF signatures can be considered to belong to category A, the most common category, of the DF classification established from a statistical study based on 303 events detected by the Cluster mission.¹² Indeed, the latter study created four large categories to which DF is linked according to their magnetic field, ion density, velocity, temperature, and pressure variations during the DF crossing. Category A, the most common, corresponds to DFs with a density decrease [see Fig. 1(d)] and a temperature increase [see Fig. 1(c)] consistent with the transition between a relatively cold dense plasma at rest with respect to a hot tenuous fast moving plasma. Note that the HPCA V_N velocity is always much larger than FPI V_N [see Fig. 1(b)], confirming that FPI instrument underestimates the velocity of the earthward flow due to

AQ3

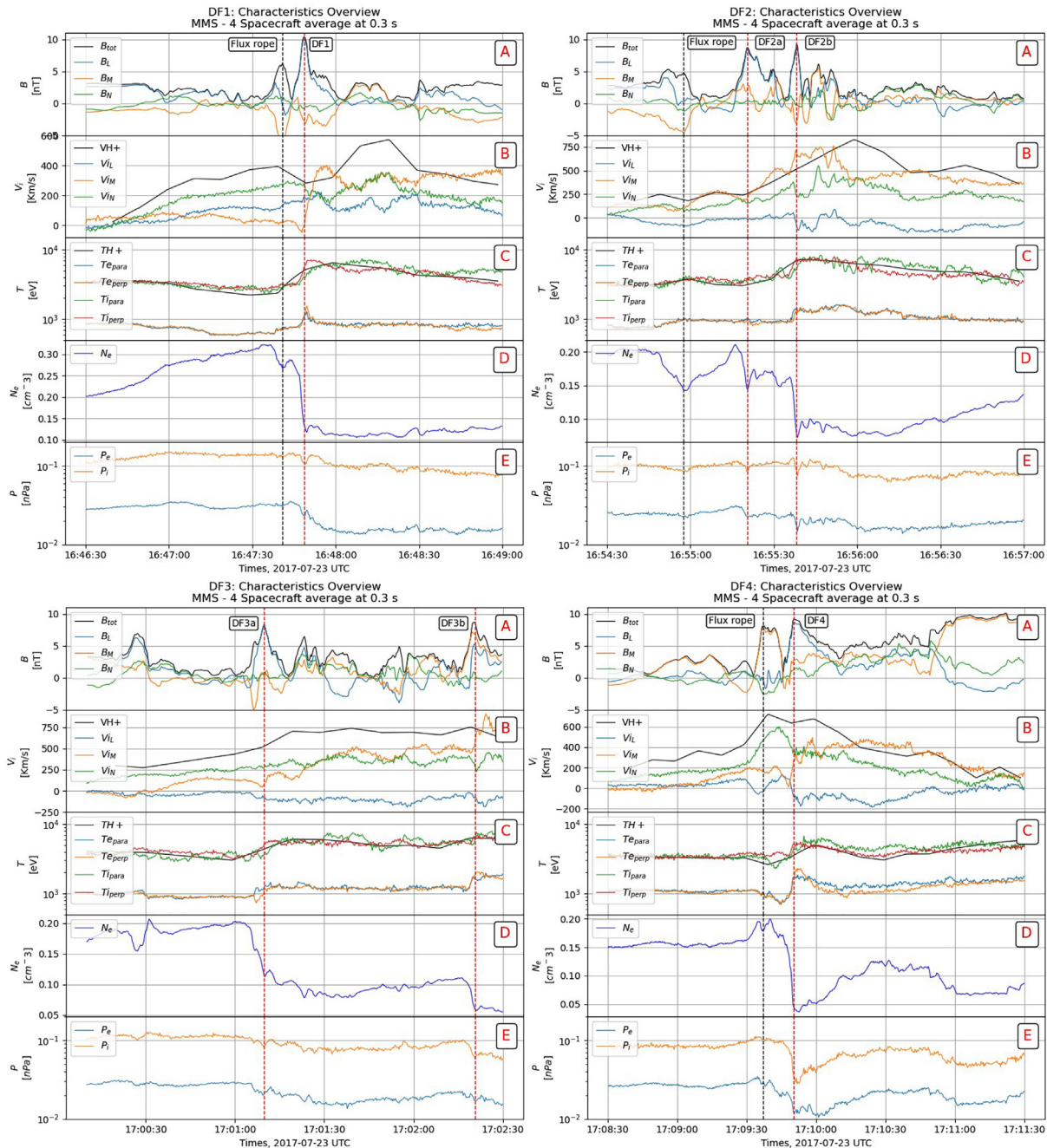


FIG. 1. Six DF signatures (vertical red dashed line) denoted DF1, DF2a,b, DF3a,b, DF4 in their respective LMN frame, all data are averaged over the four satellites then time averaged at 0.3 s. For each event, panel (a) shows the magnetic field components and its magnitude, (b) the components of ion velocity from FPI and the N component of the V_{H+} HPCA velocity, (c) the electron and ion temperatures from FPI with the isotropic proton temperature from HPCA, (d) the electron density, (e) the ion and electron pressures from FPI. Vertical black dashed lines indicate possible flux rope signatures (see text).

270 its limited upper energy. Moreover, the maximum of the V_N compo-
 271 nent of the ion velocity is always located behind the DF associated
 272 with the maximum of B_L , which according to Hamrin *et al.*¹⁹ results
 273 should, therefore, correspond to decelerated DFs with a significant

part of the energy being radiated. Furthermore, in such conditions, Fu
et al. showed that these DFs correspond to growing magnetic flux pile-
 up region (innermost flux tubes being pushed by faster outermost flux
 tubes leading to the compression of the magnetic field) causing the

TABLE I. Minimum variance analysis (MVAB) results: Eigen value ratios and vectors (in GSE).

DF	UT	$\frac{\lambda_M}{\lambda_N}$	$\frac{\lambda_L}{\lambda_N}$	L	M	N
DF1	16:47:45/16:47:50	5.69	450.62	0.14, 0.63, 0.76	0.13, -0.78, 0.62	0.98, 0.01, -0.19
DF2a	16:55:10/16:55:25	75.67	813.54	0.06, 0.47, 0.88	0.64, -0.70, 0.33	0.77, 0.54, -0.34
DF2b	16:55:35/16:55:36	19.6	14218.5	0.08, 0.72, 0.69	0.60, -0.59, 0.54	0.8, 0.37, -0.48
DF3a	17:01:03/17:01:09	42.25	103.88	0.01, 0.59, 0.81	0.61, -0.64, 0.47	0.79, 0.49, -0.36
DF3b	17:02:18/17:02:19	29.62	186.86	0.6, -0.52, 0.61	-0.20, -0.83, -0.52	0.78, 0.19, -0.60
DF4	17:09:45/17:09:52	58.12	581.82	0.32, 0.06, 0.95	0.77, -0.61, -0.22	0.56, 0.79, -0.24

TABLE II. Timing analysis results: Normal vectors and velocity (in GSE) with estimated DF thickness δ .

DF	UT	(n_x, n_y, n_z)	($V_{n_x}, V_{n_y}, V_{n_z}$)	Vn (km/s)	δ (km)	δ (d_i)
DF1	16:47:45/16:47:50	0.95, 0.30, -0.09	186, 59, -18	196	588	1.34
DF2a	16:55:10/16:55:25	0.95, 0.27, -0.13	129, 36, -17	135	811.98	1.63
DF2b	16:55:35/16:55:36	0.86, 0.17, -0.48	241, 49, -135	281	561.42	0.98
DF3a	17:01:03/17:01:09	0.60, 0.72, -0.35	289, 345, -169	481	1924.92	3.78
DF3b	17:02:18/17:02:19	0.34, 0.30, -0.89	124, 111, -327	367	587.536	0.81
DF4	17:09:45/17:09:52	0.54, 0.83, -0.14	251, 390, -63	468	1871.72	3.67

278 acceleration of electrons by the betatron effect.⁴⁷ Finally, from Fig. 279
 280 1(e), one can see that for electrons, the DF always corresponds to a
 281 transition between a high pressure to a low pressure region, whereas
 282 for the ions, it mostly corresponds to a transient pressure reduction
 283 except for DF4. Therefore, at the DF crossing, the electron pressure
 gradient can be expected to increase strongly.

284 **IV. CURRENT DENSITY AND HALL ELECTRIC FIELD**
 285 **COMPARISONS**

286 As mentioned in Sec. II, plasma conditions in the magnetotail
 287 can make the particle moment measurements difficult. One way to
 288 verify the reliability of these measurements is to compare the current
 289 densities computed from ion and electron moments averaged over the
 290 four individual spacecraft with those estimated independently from
 291 the magnetic field data at the same time resolution (0.3 s) using the
 292 curlometer technique. Figure 2 shows such comparisons for the cur-
 293 rent densities ($\mathbf{J}_{part} = en_e(\mathbf{v}_i - \mathbf{v}_e)$ vs $\mathbf{J}_{curl} = (\nabla \times \mathbf{B})/\mu_0$) and the
 294 Hall electric fields ($\mathbf{J}_{part} \times \mathbf{B}/(ne)$ vs $\mathbf{J}_{curl} \times \mathbf{B}/(ne)$) estimated for
 295 each DF event in their own LMN frame. Figures 2(a)–2(c) for each
 296 event demonstrate good agreement between the two current density
 297 measurements within an accuracy of about <10 nA/m². Indeed, con-
 298 sidering an accuracy of 0.1 nT for the magnetic field measurement,³⁷
 299 the accuracy of the current density measurements from the curlometer
 300 with a spacecraft separation of 15 km can be roughly estimated to 5
 301 nA/m². The current density accuracy from the particle measurement
 302 is estimated to 8 nA/m² (see Sec. VI for more details). In similar man-
 303 ner, Figs. 2(d)–2(f) confirm that Hall fields estimated from both cur-
 304 rents are in good agreement, within an accuracy of 1 mV/m. However,
 305 a large discrepancy between the two Hall field calculations can be
 306 found in the low density region and when current densities are smaller
 307 than or close to their error bars and oscillate around 0. In such

conditions, the error on the current density measurement is amplified 308
 by the low density and leads to a large error on the Hall field calcula- 309
 tion [e.g., Fig. 2(e), for DF4]. 310

Furthermore, we can identify each DF with their negative peak in 311
 J_M (increase in cross-tail duskward current) associated with the bipolar 312
 signature of the N component of the Hall electric field. This latter is 313
 mostly produced by the reversal of J_M just behind the DF, B_L remain- 314
 ing positive [see Figs. 2(a) and 2(b)]. This Hall field is expected due to 315
 the ion inertial scale of the DF, which leads ions to be decoupled from 316
 the magnetic field. However, its reversal seems to be related to an elec- 317
 tron scale current density shear flow at the DF or to a possible electron 318
 vortex signature. 319

320 **V. ANALYSIS OF OHM'S LAW**

The precise analysis of all terms in the generalized Ohm's law, 321
 estimated from *in situ* measurements, allows us to identify the regions 322
 where the plasma decouples from the magnetic field and kinetic effects 323
 become important. It also leads to a better understanding of which 324
 term plays the most important role in the energy conversion process. 325
 Previous analyses related to fast plasma flows in the magnetotail have 326
 been carried out using measurements from the four Cluster satellites 327
 (4 s time resolution).⁴⁸ The authors suggested that anomalous resistiv- 328
 ity term arising from electromagnetic field fluctuations and Hall term 329
 played a dominant role in the breakdown of the frozen-in condition. 330
 Using both single and multi-satellite methods, it was confirmed that 331
 Hall and electron pressure gradient terms contribute to ion decoupling 332
 at DF although Hall term was indeed dominant.¹⁴ High time and spa- 333
 tial MMS resolutions allow analysis of Ohm's law at kinetic scales, 334
 which are relevant at DF.^{21,22} Assuming a possible anomalous resistiv- 335
 ity η for collisionless plasmas, the generalized Ohm's law is written as 336

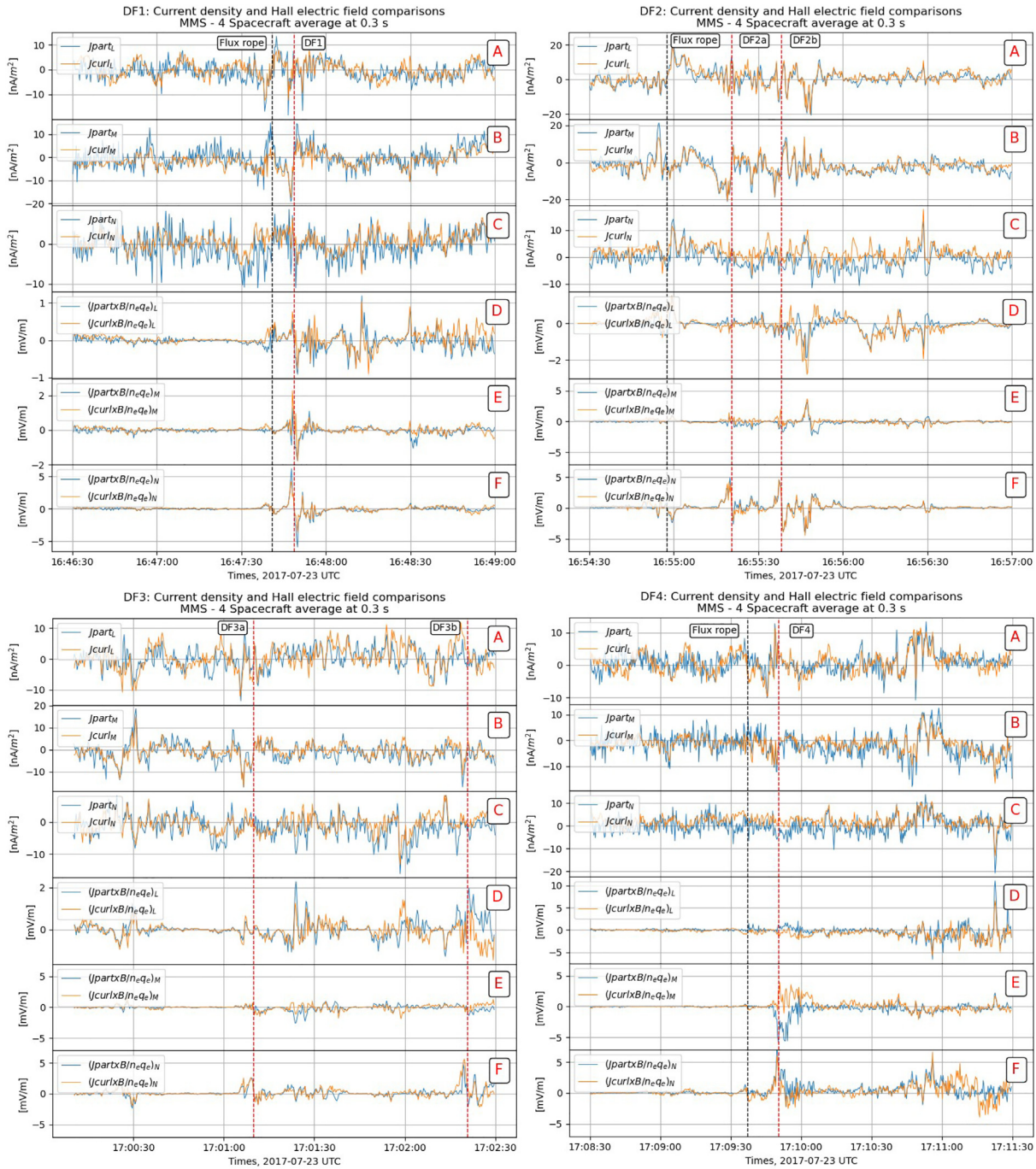


FIG. 2. For each DF event in its respective LMN frame, comparison between current densities calculated by using $\mathbf{J}_{part} = en_e(\mathbf{v}_i - \mathbf{v}_e)$ and $\mathbf{J}_{curl} = \nabla \times \mathbf{B} / \mu_0$: (a) along L, (b) along M, (c) along N, and Hall electric field comparison between two computations $\mathbf{J}_{part} / (en_e)$ and $\mathbf{J}_{curl} / (en_e)$: (d) along L, (e) along M, and (f) along N.

$$\mathbf{E} + \mathbf{v}_e \times \mathbf{B} = -\frac{1}{en} \nabla \cdot \mathbf{P}_e - \frac{m_e}{e} \frac{d\mathbf{v}_e}{dt} + \eta \mathbf{J}, \quad (1)$$

$$\mathbf{E} + \mathbf{v}_i \times \mathbf{B} = \frac{\mathbf{J} \times \mathbf{B}}{en} - \frac{1}{en} \nabla \cdot \mathbf{P}_e - \frac{m_e}{e} \frac{d\mathbf{v}_e}{dt} + \eta \mathbf{J}, \quad (2)$$

337 where \mathbf{v}_e , \mathbf{P}_e are the electron velocity and pressure tensor, respectively.
 338 One writes equivalently

where \mathbf{v}_i is the ion velocity. 339

In the dayside region, where the plasma density is on average 340
 larger than in the magnetotail and at the vicinity of the electron 341

diffusion region, all terms can be estimated with good accuracy and the validity of the Ohm's law can be tested. Pressure gradient and inertial terms are found to have significant contributions without excluding the existence of an anomalous resistivity term due to high-frequency electric field fluctuations.⁴⁹ In the low density magnetotail (<1 part-cm⁻³) and in the vicinity of DFs, electron pressure gradient and inertial terms are difficult to estimate and quite noisy even after time averaging.²² For each DF event, we have computed both terms. The inertial term is negligible, whereas the divergence of the electron pressure tensor is larger, but still very noisy. Therefore, in the rest of the study, only convective and Hall terms are shown. No anomalous resistivity will be considered, yet the electron pressure gradient term will be estimated by a single satellite method. All data are averaged over the four satellites.

Figure 3 shows the comparison between the ideal ion frozen-in ($\mathbf{E} + \mathbf{v}_i \times \mathbf{B}$) and the Hall electric field ($\mathbf{J}_{part} \times \mathbf{B}/(en)$) terms in LMN coordinates. For all events, ions are decoupled in the vicinity of the DF by the Hall electric field. However, the difference between the two terms can exceed 2 mV/m, which suggests that electron pressure gradient term is not negligible in these regions despite the difficulty to estimate it from the four satellite measurements.

Figure 4 shows the comparison between the ideal electron frozen-in term ($\mathbf{E} + \mathbf{v}_e \times \mathbf{B}$) and the ideal ion frozen-in plus the Hall term computed from curlometer ($\mathbf{E} + \mathbf{v}_i \times \mathbf{B} - \mathbf{J}_{curl} \times \mathbf{B}/(en)$). One can see that electrons are mostly magnetized as the ideal frozen-in term does not exceed 1.7 – 2 mV/m, which is the order of the error bar of the E' measurement (see Sec. VI for details about the error bars). However, at the DF, this term is very close to or exceeds the error bar. This suggests that electrons could be decoupled from the magnetic field. It is difficult to confirm that this decoupling is due to the larger pressure gradient at DF since the calculation of the divergence of the electron pressure tensor is very noisy for such low density plasma conditions.^{21,22}

However, single satellite methods can be applied to estimate the possible effect of the electron pressure gradient term at the DF.^{14,21} Using the DF velocity obtained from the timing analysis, one can consider that the time variations of the pressure in the spacecraft frame along the normal direction are mostly due to the normal pressure gradient: $\partial P_e/\partial t \sim V_{DF} \partial P_e/\partial N$. Figures 3(c) and 4(c) show this calculation (green line) based on four spacecraft averaged quantities. These figures confirm that the electron pressure gradient term is small but not negligible compared to the ideal frozen-in and Hall field terms. Note that for DF2a and DF2b (respectively, DF3a and DF3b), we have used the smallest estimated V_N . Therefore, the gradient term is overestimated for the fastest DFs (see Table II). At the vicinity of the DF crossing and along the normal direction, this raw estimate allows us to suggest that the departure between the ion frozen-in term and the Hall field (3C) and the non-zero electron frozen-in term (4C) are caused by the electron pressure gradient.

VI. ENERGY CONVERSION PROCESS AT THE DF

The energy conversion processes can be studied by computing the $\mathbf{j} \cdot \mathbf{E}$ term present in the electromagnetic energy conservation equation.⁵⁰ The $\mathbf{j} \cdot \mathbf{E}$ term governs the exchanges between electromagnetic and kinetic (thermal and bulk flow) energies in the laboratory or spacecraft frames. Positive values correspond to a load, whereas

negative values correspond to a generator.^{20,36,50} Figure 5 shows the magnetic and the electric field components, and the current density components computed from particle measurements and the corresponding $\mathbf{j} \cdot \mathbf{E}$ term for each DF event. For all DF events, the DF is associated with a positive $\mathbf{j} \cdot \mathbf{E}$ slightly ahead or at the DF, therefore, to an energy transfer from fields to the plasma (dissipation) in the spacecraft frame. However, a negative value with an equivalent amplitude is measured immediately behind the front, indicating an energy transfer from the plasma to the electromagnetic field. When we calculate separately the three terms of the scalar product using the LMN coordinates, we can see that the main contribution comes from the cross-tail current and electric field components ($J_M \cdot E_M$, not shown). Furthermore, the negative part of the energy conversion term is mostly due to the local reversal of the J_M component while E_M related to the flow motion remains positive. Note that the large variations of E_N at the DF do not lead to any energy conversion as they correspond to the Hall field, therefore, which are perpendicular to the current. Regardless of the sign, energy conversion values range from -0.02 to $+0.02$ nW/m³ except for a maximum negative value of -0.04 for DF1. Finally, one can notice that the possible flux rope signatures are associated with positive or negative energy conversion terms comparable to those associated with the DF.

The measurement of the energy conversion for a two fluid plasma quantified by $\mathbf{j} \cdot \mathbf{E}'$ (where \mathbf{E}' is the electric field in the ion or electron fluid frames) must be the same in the electron frame ($\mathbf{j} \cdot (\mathbf{E} + \mathbf{v}_e \times \mathbf{B})$) and in the ion frame ($\mathbf{j} \cdot (\mathbf{E} + \mathbf{v}_i \times \mathbf{B})$). The energy conversion process does not depend on the specific fluid frame. Furthermore, it is also mathematically constrained as $\mathbf{j} \cdot (\mathbf{E} + \mathbf{v}_i \times \mathbf{B}) - \mathbf{j} \cdot (\mathbf{E} + \mathbf{v}_e \times \mathbf{B}) = \mathbf{j} \cdot (\mathbf{j}/(en) \times \mathbf{B}) = 0$.^{21,33} Hence, this equality can also serve as a cross check of the reliability of our calculation of the energy conversion term $\mathbf{j} \cdot \mathbf{E}'$.

For each DF, Figs. 6(a) and 6(b) display four spacecraft averaged values of $[\mathbf{j} \cdot (\mathbf{E} + \mathbf{v}_e \times \mathbf{B})]$ and $[\mathbf{j} \cdot (\mathbf{E} + \mathbf{v}_i \times \mathbf{B})]$ using the current density estimated from the curlometer and from the particle measurements. We can, therefore, verify that the energy conversion term is equal in the ion and electron frames, attesting to the reliability of the energy conversion term calculation. In the fluid frames, the four spacecraft average of the energy conversion term is mostly negative (from -0.02 to -0.01 nW/m³) just ahead of the DF and corresponds to an energy transfer from the plasma to the electromagnetic fields (generator or wave radiation) in accordance with a previous MMS single event study.²¹ One can notice that, when the curlometer is used, some discrepancies between calculations in ion and electron frames can be seen for DF4. This is due to the fact that some of the current density components are smaller or close to their error bars [e.g., J_N in Fig. 2(c) for DF4] as mentioned in Sec. IV.

For each DF event, Fig. 6(c) shows the energy conversion term for each individual satellite in electron frames. These single satellite calculations indicate that the energy conversion process is not homogeneous at the scale of the tetrahedron (electron scales). Indeed, strong variations of the sign and the amplitude of the energy conversion term are seen from one satellite to another. Such variations suggest that a physical process is going on at the electron scales while the DF is propagating earthward.

For a better understanding of the origin of the non-homogeneity of the energy conversion at the electron scales, we estimated the standard deviation for each component of the current density and the

AQ4

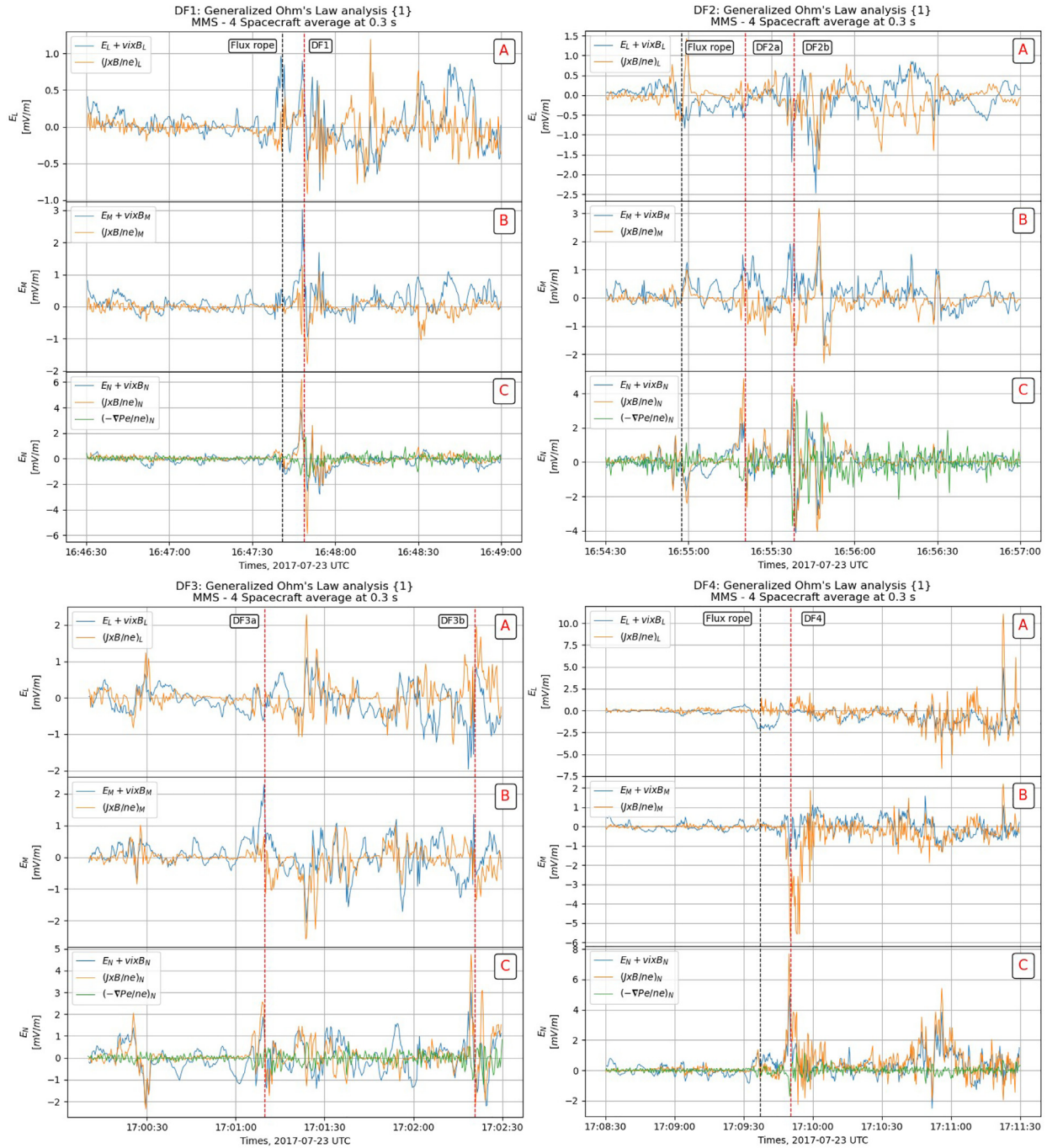


FIG. 3. Panels (a)–(c) show L , M , N components of Ohm's Law terms, respectively: $\mathbf{E} + \mathbf{v}_i \times \mathbf{B}$ (blue line), $(\mathbf{J}_{part} \times \mathbf{B})/(ne)$ (orange line). Panel (c) also includes electron pressure gradient term along N (green line).

455 electric field in the fluid frame ($\mathbf{E}' = \mathbf{E} + \mathbf{v}_e \times \mathbf{B}$) normalized by their
 456 respective error bar: $SD(X)/\Delta X = \sqrt{\sum_{i=1}^4 (X_i - \langle X \rangle)^2 / 4} / \Delta X$,
 457 $\langle X \rangle$ being the four spacecraft average of the X component and ΔX its

458 respective estimated error bar. For the electric field, we use the error
 459 bar provided by the EDP team (~ 1 mV/m),³⁹ whereas for the electron
 460 convective term, the error is estimated as $(\Delta V_e B + V_e \Delta B)$ with
 461 $\Delta B = 0.1$ nT³⁷ and using the moment error bars provided by the FPI

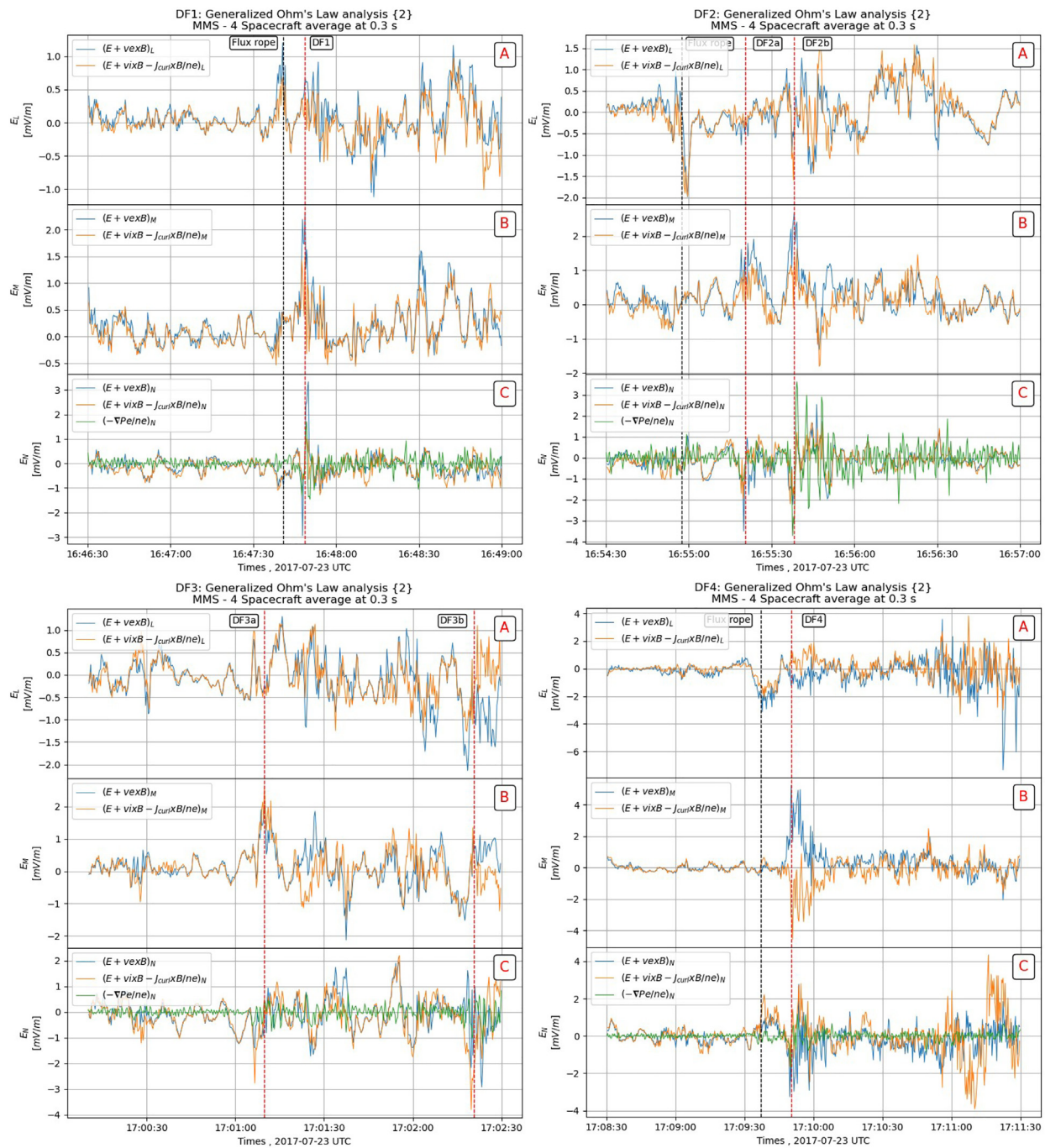


FIG. 4. Panels (a)–(c) show L , M , N components of Ohm's Law terms, respectively: $E + \mathbf{v}_e \times \mathbf{B}$ (blue line), and $E + \mathbf{v}_i \times \mathbf{B} - (\mathbf{J}_{\text{curl}} \times \mathbf{B}) / (ne)$ (orange line). Panel (c) also includes electron pressure gradient term along N (green line).

462 team.⁴¹ Thus, we found that the error bar of E' averaged over each DF
 463 period is $\sim 1.7 - 2$ mV/m. For the error bar of the current density
 464 $\Delta J_{\text{part}} = e \cdot (\Delta N_e) \cdot (V_i - V_e) + e \cdot N_e \cdot (\Delta V_i + \Delta V_e)$, we got an
 465 average value ~ 8 nA/m². Let us remember that in the present study,

we use the partial moments, which allow us to deal with smaller errors.

Figures 7(a)–7(c) and 8(a)–8(c) show for each DF, the three components of the current density and the electric field (E'), respectively.

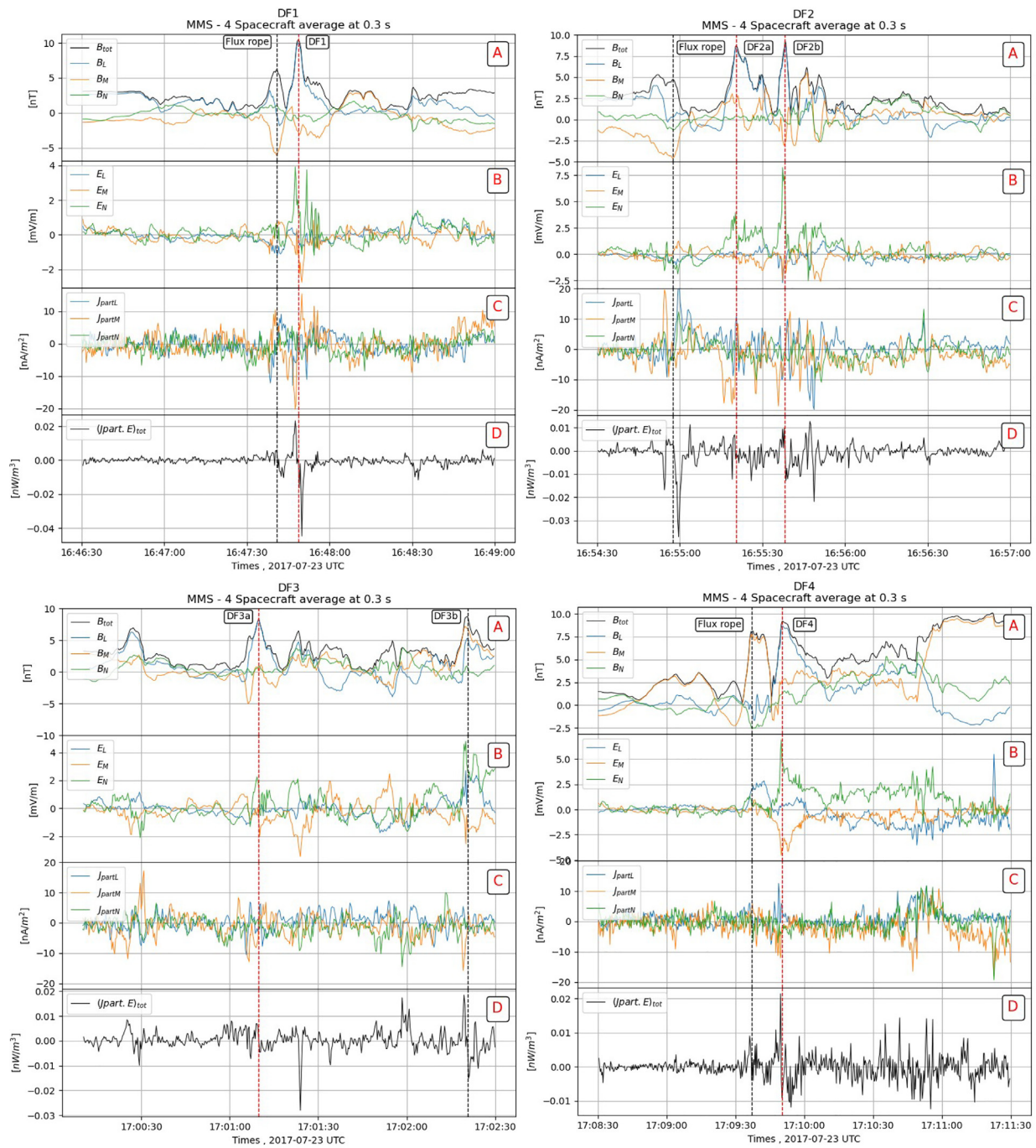


FIG. 5. For each DF event and in LMN frame: (a) magnitude and components of the magnetic field, (b) electric field components, (c) current density components using J_{part} , and (d) energy conversion $j_{part} \cdot E$ (in the spacecraft frame).

470 Figures 7(d), 7(e), 8(d), and 8(e) show the raw and normalized SD of
 471 the corresponding quantity. One can see that at DFs, the normalized
 472 SD of the electric field (E') is usually greater (≥ 1) than the normalized
 473 SD of the current density (< 1). These results are consistent with the

fact that the dispersion between the four curves measured by the four 474
 satellites is usually smaller for the current density than for the electric 475
 field (E') [Figs. 7(a)–7(c) and 8(a)–8(c)]. Therefore, the non- 476
 homogeneity of the energy conversion process seems to be caused 477

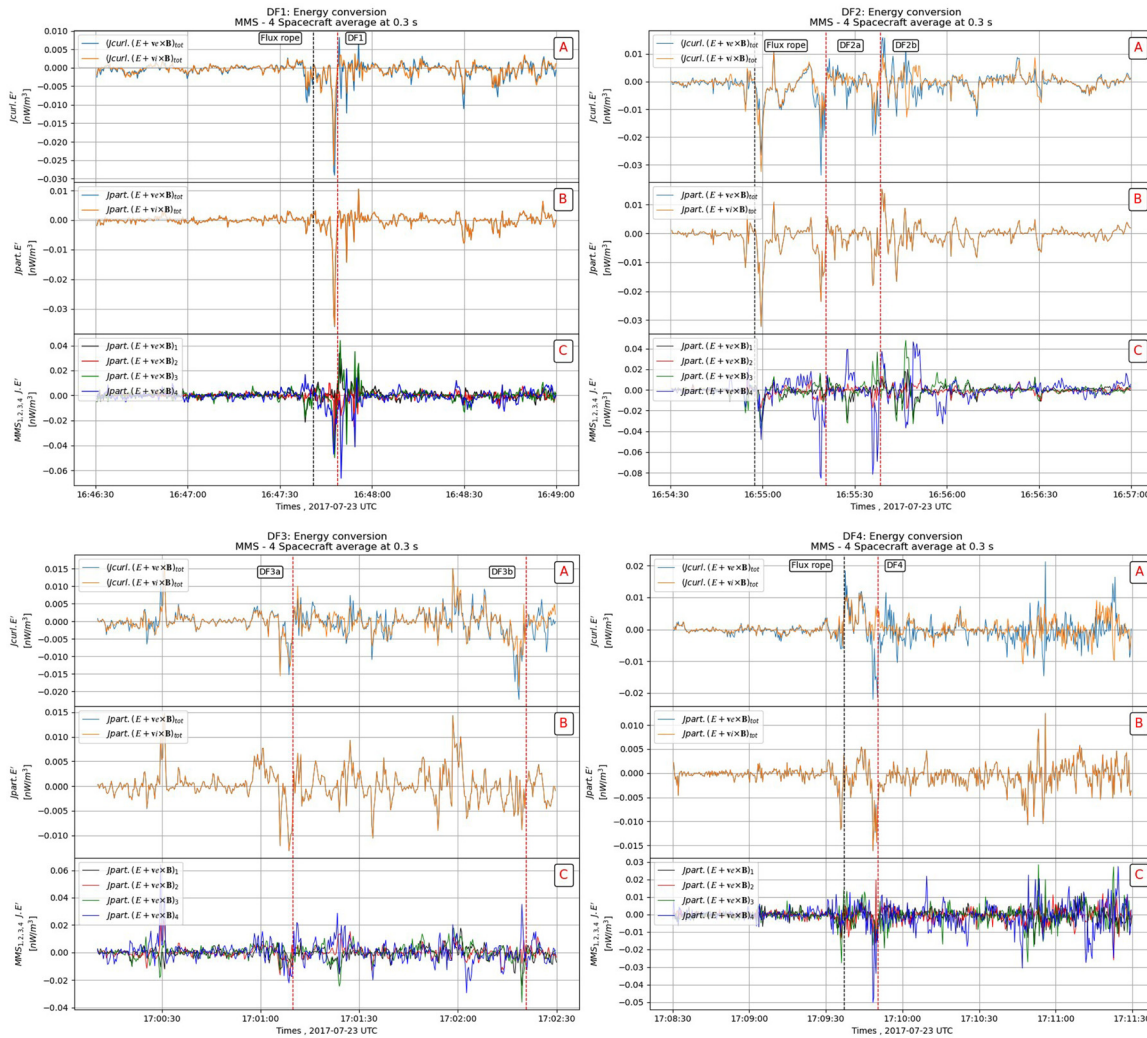


FIG. 6. Comparison of the energy conversion term in both electron and ion frames. (a) Four spacecraft average of the energy conversion using J_{curl} . (b) Four spacecraft average of the energy conversion using J_{part} . (c) Energy conversion using J_{part} for MMS1 (black), MMS2 (red), MMS3 (green), and MMS4 (blue).

478 mainly by the electric fluctuations having electron scales. Conversely, 479 the current density remains more homogeneous at the scale of the 480 MMS tetrahedron, which suggests that the origin of the electric field 481 fluctuations is mostly electrostatic as we will discuss in Sec. VII.

482 VII. DISCUSSION AND SUMMARY

483 Six DF events embedded in fast earthward flows and detected 484 during a large scale substorm event have been analyzed in the present 485 study. These DF events belong to the most common category corre- 486 sponding to a decrease in the density and an increase in the tempera- 487 ture;¹² therefore, they are characterized by a transition between a cold 488 dense plasma at rest to a hot tenuous accelerated plasma moving 489 earthward. We analyzed each front orientation using the MVAB 490 method as well as a timing analysis and found that all DFs are mostly 491 moving earthward with some DFs having a significant duskward and

southward motions. We have pointed out that the HPCA V_N velocity 492 is always much larger than FPI V_N s, confirming that FPI instrument 493 underestimates the velocity of the earthward flow in the magnetotail 494 due to its low upper energy. This caveat is quite common during sub- 495 storm events as the plasma is energized due to the global magnetotail 496 reconfiguration. Moreover, the maximum of the V_N component of the 497 ion velocity is always located behind the DF associated with the maxi- 498 mum of B_z , which, according to a statistical study based on Cluster 499 data, should correspond to decelerated DFs with a significant part of 500 the energy being radiated (in the spacecraft frame).^{19,47} In order to 501 have more confidence on the particle moment measurements, we have 502 compared the current densities obtained from the particle instruments 503 (using partial moment for electrons) with those obtained from the 504 curlometer technique. Despite relatively small values (<20 nA/m²) 505 associated with the DF crossing, we found a good agreement between 506

AQ5

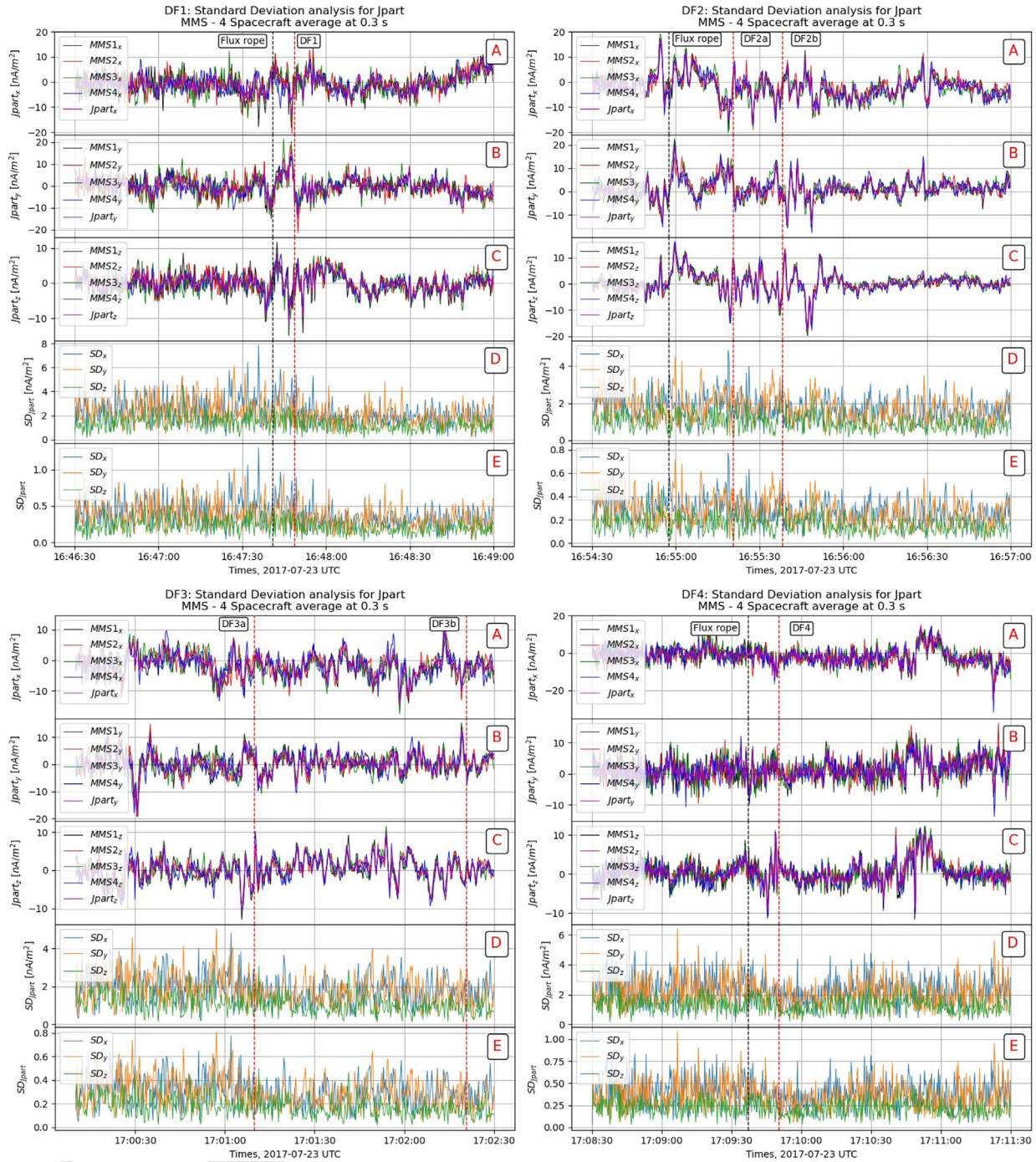


FIG. 7. Components of the current density obtained from FPI in GSE for each MMS satellite and the four spacecraft average [panels (a)–(c)]. Panel D shows the standard deviation $SD(j)$ of each component of the current density. Panel E shows the $SD(j)$ normalized by the current density error bar, see text for details.

507 the two types of current density estimates. Then, to better understand
 508 ion and electron dynamics at the DF crossing, we analyzed Ohm’s law.
 509 Near the DF crossing, we found that ions are decoupled from the mag-
 510 netic field due to the Hall field. A clear bipolar signature of the Hall

field is present normal to the DF (along N) mostly related to a reversal 511
 of the cross-tail current just behind the DF. However, the Hall field 512
 does not seem to be sufficient to explain the full decoupling of the 513
 ions. The electron pressure gradient term is also likely involved in this 514

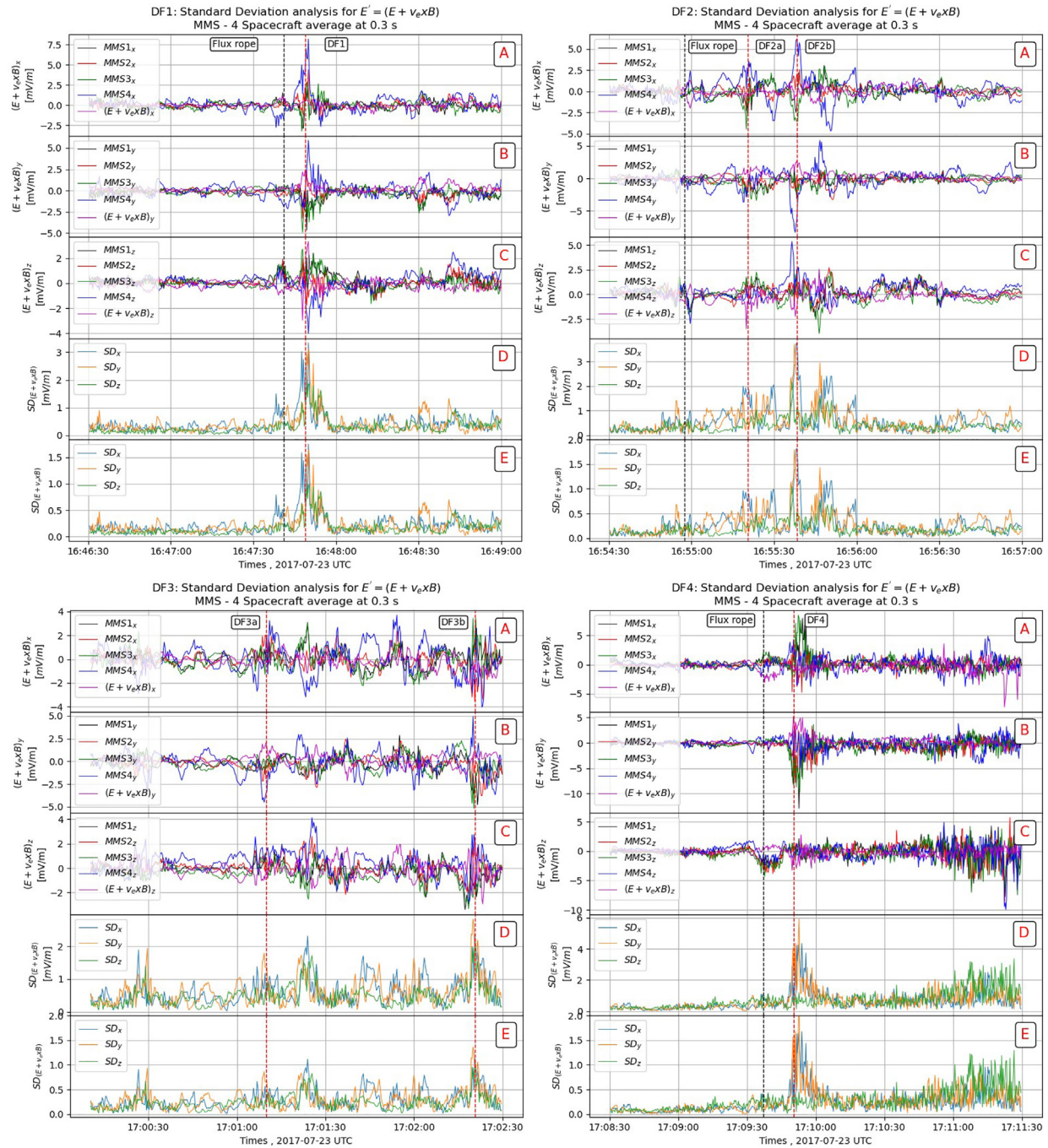


FIG. 8. Same as Fig. 7 for the electric field in the electron frame ($E' = E + V_e \times B$). Panel E shows the standard deviation normalized by the error bar of E' , see text for details.

515 decoupling. Due to the low plasma density, we could not compute the
 516 divergence of the electron pressure tensor with a sufficient reliability.
 517 Instead, we used single satellite method (applied to the four spacecraft
 518 averaged data) to estimate the electron pressure gradient along the

normal direction.^{14,21} For most of the DF events, we found that the
 signature of the electron pressure gradient along the normal is consistent
 with a significant contribution to the ion decoupling and could account
 for the departure between the ideal ion frozen-in term

523 $(\mathbf{E} + \mathbf{v}_i \times \mathbf{B})$ and the Hall field. Electrons are magnetized most of the
524 time. However, at the DF crossing, the departure between the electron
525 ideal frozen-in term $(\mathbf{E} + \mathbf{v}_e \times \mathbf{B})$ is very close to or exceeds the error
526 bar, which also suggests, as for the ions, that the electron pressure
527 term along the normal can take part in the electron decoupling. In the
528 other directions (L and M), it is not possible to estimate the gradient
529 by the same technique. However, the results obtained along the normal
530 suggest that the decoupling along L and M also involves the elec-
531 tron pressure term in these directions.

532 In order to investigate the energy conversion process at the DF,
533 we have estimated the $\mathbf{j} \cdot \mathbf{E}$ term.^{17,19–22,26,51} For all DFs in the space-
534 craft frame, we found that the energy is transferred from the electro-
535 magnetic field to the plasma (dissipation or loading) at or just ahead
536 of the DF and from the plasma to the electromagnetic field behind the
537 DF (wave radiation or generator). The amplitudes of the positive and
538 negative peaks have similar values ($\pm 0.02 \text{ nW}\cdot\text{m}^{-3}$), which do not
539 allow us to draw conclusions about a net energy transfer between fields
540 and particles, despite the fact that the normal velocity peak is detected
541 behind the front.^{19,47} This reversal of the energy conversion is mostly
542 related to the reversal of the cross-tail current component (J_M) just
543 behind the front. Such a current reversal at the DF has been already
544 mentioned by Yao *et al.* based on 2003 Cluster data (subproton scale
545 spacecraft separation $\sim 200 \text{ km}$) but only related to DFs preceded by a
546 dip of the magnetic field.⁴⁶ It has been also recently mentioned by Liu
547 *et al.* in a previous MMS single DF case study event leading to a nega-
548 tive $\mathbf{j} \cdot \mathbf{E}$ behind the DF. The origin of this reversal is not fully under-
549 stood and could be due to a current density shear at an electron scale
550 between the main front and the front trailing part. Another possibility
551 could be the formation of substructures, such as electron vortices
552 driven by the current carried by electrons within the front region,
553 which could contribute locally to the increase in the total magnetic
554 field.⁵² The existence of such structures within the ion scale DF struc-
555 ture needs to be confirmed by further studies. Whatever the origin of
556 these current density reversals, these results suggest that DFs have
557 complex substructures that make difficult to draw conclusions about
558 the net energy transfer in the spacecraft frame.

559 To better understand this energy conversion process, we have
560 carried out the computation in each fluid frame (ion and electron)
561 using four spacecraft average value of \mathbf{E}' and \mathbf{j} . Equality of the calcula-
562 tion in both ion and electron frames has been used as a reliability test.
563 In these fluid frames, the $\mathbf{j} \cdot \mathbf{E}'$ just ahead of the DF is negative most of
564 the time indicating a net transfer from the plasma to the electromag-
565 netic fields as also found in a previous MMS single DF event.²¹
566 Therefore, the energy would be radiated and this process should lead
567 to the deceleration of the fast plasma flow. Note that this negative
568 term cannot be related to the electron pressure gradient along the nor-
569 mal since this latter is perpendicular to the main current J_M . However,
570 as we mentioned in Sec. V, the electron decoupling along M can also
571 be due to the electron pressure gradient along this direction and leads
572 to negative $\mathbf{j} \cdot \mathbf{E}' \sim J_M E'_M = -J_M \cdot |\nabla P_e|_M / (en)$.

573 Furthermore, we have analyzed the homogeneity of this energy
574 conversion process by computing the $\mathbf{j} \cdot \mathbf{E}'$ term for each satellite. We
575 found that the energy conversion is not homogeneous at the scale of
576 the tetrahedron, i.e., at the electron scales. By computing the standard
577 deviation of \mathbf{E}' and \mathbf{j} normalized by their respective error bars, we
578 showed that the non-homogeneity of the energy conversion process
579 comes mostly from the electric field fluctuations while the

580 contribution of current density fluctuations is smaller. As mentioned
581 above, these electric field fluctuations should be related to the electron
582 pressure gradient. This result is consistent with previous studies, which
583 identified large amplitude electric field fluctuations related to lower-
584 hybrid drift waves from space observations.^{22–26} It is also consistent
585 with 3D PIC simulations.^{30,33,34} These waves with frequencies between
586 ion and electron gyrofrequencies ($f_{ci} < f < f_{ce}$) are expected to be gen-
587 erated by the large density gradient ($n_e / \nabla n_e \sim c / \omega_{pi}$) at DF and are
588 known to have wavelengths on the order of the electron Larmor radius
589 for the fastest growing mode.^{53,54} These electron-scale wavelengths
590 correspond to the average spacecraft separation for these events, and
591 the period of the LHD waves is much smaller than the DF crossing
592 time. These waves are able to generate ripples on the front at the
593 electron scales, which can lead to the non-homogeneity of the energy
594 conversion process.²⁷ Indeed, these waves are considered as “quasi-
595 electrostatic” waves. Due to their frequency range, ions can be
596 assumed unmagnetized, whereas electrons are magnetized.⁵⁴
597 Therefore, electron drift in the electric field of the waves produces
598 small perpendicular (to the background magnetic field) currents and a
599 parallel magnetic field perturbations causing the ripple of the front at
600 electron scales. These currents are much smaller than the current asso-
601 ciated with the front. Thus, regarding the energy conversion process in
602 the fluid frame ($\mathbf{J} \cdot \mathbf{E}'$), the dominant term corresponds to the product
603 between the ion-scale current associated with the front (\mathbf{J}_0) and the
604 electron-scale electric field associated with the LHD waves ($\delta \mathbf{E}'$). The
605 energy conversion ($\delta \mathbf{J} \cdot \delta \mathbf{E}'$) due to currents generated by LHD waves
606 ($\delta \mathbf{J}$) is smaller and can be considered as a second order contribution
607 compared to the former term. This can be summarized as $\mathbf{J} \cdot \mathbf{E}'$
608 $\simeq \mathbf{J}_0 \cdot \delta \mathbf{E}'$ with $\delta \mathbf{J} \cdot \delta \mathbf{E}' \ll \mathbf{J}_0 \cdot \delta \mathbf{E}'$. The non-linear evolution of these
609 waves could generate electron scale vortices⁵⁵ that could explain the
610 current density reversal behind the DF and the negative part of $\mathbf{j} \cdot \mathbf{E}$
611 although the low inhomogeneity of the current density at the scale of
612 the tetrahedron is not in favor of this interpretation.

613 However, from their 3D PIC simulations, Nakamura *et al.* found
614 an oscillating $\mathbf{j} \cdot \mathbf{E}'$, which once integrated along the cross-tail direction
615 leads to a non-zero positive term corresponding to an energy dissipa-
616 tion.³⁴ The detailed characterization of the wave activity associated
617 with these DF is beyond the scope of the present study and left for a
618 further investigation. However, our results support the fact that the
619 non-homogeneity of the energy conversion process at the electron
620 scales is likely due to the electric field fluctuations of the lower-hybrid
621 drift instability that develops in the vicinity of the DF due to the large
622 density gradient; this density gradient being due to a combined effect
623 of the tangential nature of the DF and the propagation of a tenuous
624 (and hot) plasma through a denser (and colder) plasma at rest. The
625 present study also confirms the need for a three-dimensional analysis
626 of the energy conversion process at the DF as the lower-hybrid drift
627 waves causing the electron scale variations of the front propagate in
628 the direction perpendicular to density gradient, therefore, perpendicu-
629 lar to the direction of the fast plasma flow.^{24,26} The net energy transfer
630 at DF needs not only to be investigated and integrated along the direc-
631 tion of the plasma flow but also perpendicularly to the DF density gra-
632 dient. Therefore, the role of DF in the global energy cycle of the
633 Earth's magnetosphere still needs further investigation and in particu-
634 lar statistical studies focused on the energy conversion process at DF
635 need to take into account these electron scale substructures. Indeed,
636 the positive than negative $\mathbf{J} \cdot \mathbf{E}$ terms at and behind the DF,

637 respectively, confirm that DFs play an important role in this cycle.
 638 Their contribution is not only related to a local dissipative effect (at
 639 DF) but also to the generation of electromagnetic fields (just behind
 640 the DF). This latter contribution can be (i) associated with the emis-
 641 sion of waves that can transport energy to other regions (e.g., auroral
 642 region) and interact with the particles causing their acceleration or (ii)
 643 associated with the formation of coherent electromagnetic structures,
 644 such as kinetic-scale vortices that can contribute to and modify the
 645 energy and plasma transport.^{58,59}

AQ6

647 **ACKNOWLEDGMENTS**

648 The authors thank the entire MMS team for providing data
 649 publicly available from the MMS Science Data Center ([http://](http://lasp.colorado.edu/mms/sdc/public/)
 650 lasp.colorado.edu/mms/sdc/public/) and the SPEDAS software
 651 team⁵⁶ in particular E. Grimes for pyspedas effort developments. S.
 652 W. Alqeeq's Ph.D. fellowship is supported by CNES and PAUSE
 653 program ([https://www.college-de-france.fr/site/programme-pause/](https://www.college-de-france.fr/site/programme-pause/index.htm)
 654 [index.htm](https://www.college-de-france.fr/site/programme-pause/index.htm)) and managed by CNRS.

655 **AUTHOR DECLARATIONS**

656 **Conflict of Interest**

657 The authors have no conflicts to disclose.

658 **DATA AVAILABILITY**

659 The MMS data that support the findings of this study are publicly
 660 available from the MMS Science Data Center ([http://lasp.colora-](http://lasp.colorado.edu/mms/sdc/public/)
 661 [do.edu/mms/sdc/public/](http://lasp.colorado.edu/mms/sdc/public/)), Ref. 57.

662 **REFERENCES**

663 ¹W. Baumjohann, G. Paschmann, and H. Luehr, "Characteristics of high-speed
 664 ion flows in the plasma sheet," *J. Geophys. Res.: Space Phys.* **95**, 3801–3809,
 665 <https://doi.org/10.1029/JA095IA04p03801> (1990).
 666 ²V. Angelopoulos, W. Baumjohann, C. F. Kennel, F. V. Coronti, M. G.
 667 Kivelson, R. Pellat, R. J. Walker, H. Luehr, and G. Paschmann, "Bursty bulk
 668 flows in the inner central plasma sheet," *J. Geophys. Res.: Space Phys.* **97**,
 669 4027–4039, <https://doi.org/10.1029/91JA02701> (1992).
 670 ³K. Shiokawa, W. Baumjohann, and G. Haerendel, "Braking of high-speed flows
 671 in the near-Earth tail," *Geophys. Res. Lett.* **24**, 1179–1182, [https://doi.org/](https://doi.org/10.1029/97GL01062)
 672 [10.1029/97GL01062](https://doi.org/10.1029/97GL01062) (1997).
 673 ⁴K. Shiokawa, W. Baumjohann, G. Haerendel, G. Paschmann, J. F. Fennell, E.
 674 Friis-Christensen, H. Lühr, G. D. Reeves, C. T. Russell, P. R. Sutcliffe, and K.
 675 Takahashi, "High-speed ion flow, substorm current wedge, and multiple Pi 2
 676 pulsations," *J. Geophys. Res.: Space Phys.* **103**, 4491–4508, [https://doi.org/](https://doi.org/10.1029/97JA01680)
 677 [10.1029/97JA01680](https://doi.org/10.1029/97JA01680) (1998).
 678 ⁵M. I. Sitnov, M. Swisdak, and A. V. Divin, "Dipolarization fronts as a signature
 679 of transient reconnection in the magnetotail," *J. Geophys. Res.: Space Phys.*
 680 **114**, A04202 (2009).
 681 ⁶J. F. Drake, M. Swisdak, P. A. Cassak, and T. D. Phan, "On the 3-D structure
 682 and dissipation of reconnection-driven flow bursts," *Geophys. Res. Lett.* **41**,
 683 3710–3716, <https://doi.org/10.1002/2014GL060249> (2014).
 684 ⁷H. S. Fu, J. B. Cao, Y. V. Khotyaintsev, M. I. Sitnov, A. Runov, S. Y. Fu, M.
 685 Hamrin, M. André, A. Retinò, Y. D. Ma, H. Y. Lu, X. H. Wei, and S. Y. Huang,
 686 "Dipolarization fronts as a consequence of transient reconnection: *In situ*
 687 evidence," *Geophys. Res. Lett.* **40**, 6023–6027, [https://doi.org/10.1002/](https://doi.org/10.1002/2013GL058620)
 688 [2013GL058620](https://doi.org/10.1002/2013GL058620) (2013).
 689 ⁸P. L. Pritchett and F. V. Coroniti, "A kinetic ballooning/interchange instability
 690 in the magnetotail," *J. Geophys. Res.: Space Phys.* **115**, A06301 (2010).
 691 ⁹D. H. Pontius, Jr. and R. A. Wolf, "Transient flux tubes in the terrestrial mag-
 692 netosphere," *Geophys. Res. Lett.* **17**, 49–52, [https://doi.org/10.1029/](https://doi.org/10.1029/GL017i001p00049)
 693 [GL017i001p00049](https://doi.org/10.1029/GL017i001p00049) (1990).

AQ8

¹⁰S.-I. Ohtani, M. A. Shay, and T. Mukai, "Temporal structure of the fast convec-
 694 tive flow in the plasma sheet: Comparison between observations and two-fluid
 695 simulations," *J. Geophys. Res.: Space Phys.* **109**, A03210 (2004).
 696 ¹¹A. Runov, V. Angelopoulos, M. I. Sitnov, V. A. Sergeev, J. Bonnell, J. P.
 697 McFadden, D. Larson, K.-H. Glassmeier, and U. Auster, "THEMIS observations
 698 of an earthward-propagating dipolarization front," *Geophys. Res. Lett.* **36**,
 699 L14106, <https://doi.org/10.1029/2009GL038980> (2009).
 700 ¹²D. Schmid, R. Nakamura, F. Plaschke, M. Volwerk, and W. Baumjohann, "Two
 701 states of magnetotail dipolarization fronts: A statistical study," *J. Geophys. Res.:*
 702 *Space Phys.* **120**, 1096–1108, <https://doi.org/10.1002/2014JA020380> (2015).
 703 ¹³J. Liu, V. Angelopoulos, A. Runov, and X.-Z. Zhou, "On the current sheets sur-
 704 rounding dipolarizing flux bundles in the magnetotail: The case for wedgelets,"
 705 *J. Geophys. Res.: Space Phys.* **118**, 2000–2020, [https://doi.org/10.1002/](https://doi.org/10.1002/jgra.50092)
 706 [jgra.50092](https://doi.org/10.1002/jgra.50092) (2013).
 707 ¹⁴H. S. Fu, Y. V. Khotyaintsev, A. Vaivads, M. André, and S. Y. Huang, "Electric
 708 structure of dipolarization front at sub-proton scale," *Geophys. Res. Lett.* **39**,
 709 L06105, <https://doi.org/10.1029/2012GL051274> (2012).
 710 ¹⁵Y. V. Khotyaintsev, C. M. Cully, A. Vaivads, M. André, and C. J. Owen,
 711 "Plasma jet braking: energy dissipation and nonadiabatic electrons," *Phys. Rev.*
 712 *Lett.* **106**, 165001 (2011).
 713 ¹⁶H. Fu, E. E. Grigorenko, C. Gabrielse, C. Liu, S. Lu, K. J. Hwang, X. Zhou, Z.
 714 Wang, and F. Chen, "Magnetotail dipolarization fronts and particle accelera-
 715 tion: A review," *Sci. China Earth Sci.* **63**, 235–256 (2020).
 716 ¹⁷V. Angelopoulos, A. Runov, X. Z. Zhou, D. L. Turner, S. A. Kiehas, S. S. Li, and
 717 I. Shinohara, "Electromagnetic energy conversion at reconnection fronts,"
 718 *Science* **341**, 1478–1482 (2013).
 719 ¹⁸C. C. Chaston, J. W. Bonnell, L. Clausen, and V. Angelopoulos, "Energy trans-
 720 port by kinetic-scale electromagnetic waves in fast plasma sheet flows,"
 721 *J. Geophys. Res.: Space Phys.* **117**, A09202 (2012).
 722 ¹⁹M. Hamrin, T. Pitkänen, P. Norqvist, T. Karlsson, H. Nilsson, M. André, S.
 723 Buchert, A. Vaivads, O. Marghitu, B. Klecker, L. M. Kistler, and I. Dandouras,
 724 "Evidence for the braking of flow bursts as they propagate toward the Earth,"
 725 *J. Geophys. Res.: Space Phys.* **119**, 9004–9018, [https://doi.org/10.1002/](https://doi.org/10.1002/2014JA020285)
 726 [2014JA020285](https://doi.org/10.1002/2014JA020285) (2014).
 727 ²⁰S. Y. Huang, H. S. Fu, Z. G. Yuan, M. Zhou, S. Fu, X. H. Deng, W. J. Sun, Y.
 728 Pang, D. D. Wang, H. M. Li, H. M. Li, and X. D. Yu, "Electromagnetic energy
 729 conversion at dipolarization fronts: Multispacecraft results," *J. Geophys. Res.:*
 730 *Space Phys.* **120**, 4496–4502, <https://doi.org/10.1002/2015JA021083> (2015).
 731 ²¹Z. H. Yao, I. J. Rae, R. L. Guo, A. N. Fazakerley, C. J. Owen, R. Nakamura, W.
 732 Baumjohann, C. E. J. Watt, K. J. Hwang, B. L. Giles, C. T. Russell, R. B. Torbert,
 733 A. Varsani, H. S. Fu, Q. Q. Shi, and X. J. Zhang, "A direct examination of the
 734 dynamics of dipolarization fronts using MMS," *J. Geophys. Res.: Space Phys.*
 735 **122**, 4335–4347, <https://doi.org/10.1002/2016JA023401> (2017).
 736 ²²C. M. Liu, H. S. Fu, Y. Xu, Y. V. Khotyaintsev, J. L. Burch, R. E. Ergun, D. G.
 737 Gershman, and R. B. Torbert, "Electron-scale measurements of dipolarization front,"
 738 *Geophys. Res. Lett.* **45**, 4628–4638, <https://doi.org/10.1029/2018GL077928> (2018).
 739 ²³V. Sergeev, V. Angelopoulos, S. Apatenkov, J. Bonnell, R. Ergun, R. Nakamura,
 740 J. McFadden, D. Larson, and A. Runov, "Kinetic structure of the sharp injection/
 741 dipolarization front in the flow-braking region," *Geophys. Res. Lett.* **36**,
 742 L21105, <https://doi.org/10.1029/2009GL040658> (2009).
 743 ²⁴A. Divin, Y. V. Khotyaintsev, A. Vaivads, and M. André, "Lower hybrid drift
 744 instability at a dipolarization front," *J. Geophys. Res.: Space Phys.* **120**,
 745 1124–1132, <https://doi.org/10.1002/2014JA020528> (2015).
 746 ²⁵O. Le Contel, R. Nakamura, H. Breuillard, M. R. Argall, D. B. Graham, D.
 747 Fischer, A. Retinò, M. Berthomier, R. Pottelette, L. Mirioni, T. Chust, F. D.
 748 Wilder, D. J. Gershman, A. Varsani, P. A. Lindqvist, Y. V. Khotyaintsev, C.
 749 Norgren, R. E. Ergun, K. A. Goodrich, J. L. Burch, R. B. Torbert, J. Needell, M.
 750 Chutter, D. Rau, I. Dors, C. T. Russell, W. Magnes, R. J. Strangeway, K. R.
 751 Bromund, H. Y. Wei, F. Plaschke, B. J. Anderson, G. Le, T. E. Moore, B. L.
 752 Giles, W. R. Paterson, C. J. Pollock, J. C. Dorelli, L. A. Avano, Y. Saito, B.
 753 Lavraud, S. A. Fuselier, B. H. Mauk, I. J. Cohen, D. L. Turner, J. F. Fennell, T.
 754 Leonard, and A. N. Jaynes, "Lower hybrid drift waves and electromagnetic elec-
 755 tron space-phase holes associated with dipolarization fronts and field-aligned
 756 currents observed by the magnetospheric multiscale mission during a sub-
 757 storm," *J. Geophys. Res.: Space Phys.* **122**, 12236–12257, <https://doi.org/10.1002/2017JA024550> (2017).
 758
 759

- 760 ²⁶J. Yang, J. B. Cao, H. S. Fu, T. Y. Wang, W. L. Liu, and Z. H. Yao, "Broadband
761 high-frequency waves detected at dipolarization fronts," *J. Geophys. Res.:
762 Space Phys.* **122**, 4299–4307, <https://doi.org/10.1002/2016JA023465> (2017).
763 ²⁷D.-X. Pan, Y. V. Khotyaintsev, D. B. Graham, A. Vaivads, X.-Z. Zhou, M.
764 André, P.-A. Lindqvist, R. E. Ergun, O. Le Contel, C. T. Russell, R. B. Torbert,
765 B. Giles, and J. L. Burch, "Rippled electron-scale structure of a dipolarization
766 front," *Geophys. Res. Lett.* **45**, 12,116–12,124, [https://doi.org/10.1029/
767 2018GL080826](https://doi.org/10.1029/2018GL080826) (2018).
768 ²⁸Z. H. Zhong, X. H. Deng, M. Zhou, W. Q. Ma, R. X. Tang, Y. V. Khotyaintsev,
769 B. L. Giles, C. T. Russell, and J. L. Burch, "Energy conversion and dissipation at
770 dipolarization fronts: A statistical overview," *Geophys. Res. Lett.* **46**,
771 12,693–12,701, <https://doi.org/10.1029/2019GL085409> (2019).
772 ²⁹L. Q. Zhang, W. Baumjohann, Y. V. Khotyaintsev, J. L. Burch, J. Webster, J. Y.
773 Wang, C. Wang, L. Dai, and C. Y. Zhang, "BBF deceleration down-tail of
774 $X < -15$ RE From MMS Observation," *J. Geophys. Res.: Space Phys.* **125**,
775 e26837 (2020).
776 ³⁰A. Divin, Y. V. Khotyaintsev, A. Vaivads, M. André, S. Markidis, and G.
777 Lapenta, "Evolution of the lower hybrid drift instability at reconnection jet
778 front," *J. Geophys. Res.: Space Phys.* **120**, 2675–2690, [https://doi.org/10.1002/
779 2014JA020503](https://doi.org/10.1002/2014JA020503) (2015).
780 ³¹Y. V. Khotyaintsev, A. Divin, A. Vaivads, M. André, and S. Markidis, "Energy
781 conversion at dipolarization fronts," *Geophys. Res. Lett.* **44**, 1234–1242, [https://
782 doi.org/10.1002/2016GL071909](https://doi.org/10.1002/2016GL071909) (2017).
783 ³²Y. Yang, W. H. Matthaeus, T. N. Parashar, C. C. Haggerty, V. Roytershteyn,
784 W. Daughton, M. Wan, Y. Shi, and S. Chen, "Energy transfer, pressure tensor,
785 and heating of kinetic plasma," *Phys. Plasmas* **24**, 072306 (2017).
786 ³³M. I. Sitnov, V. G. Merkin, V. Roytershteyn, and M. Swisdak, "Kinetic dissipation
787 around a dipolarization front," *Geophys. Res. Lett.* **45**, 4639–4647, [https://
788 doi.org/10.1029/2018GL077874](https://doi.org/10.1029/2018GL077874) (2018).
789 ³⁴T. K. M. Nakamura, T. Umeda, R. Nakamura, H. S. Fu, and M. Oka,
790 "Disturbance of the front region of magnetic reconnection outflow jets due to
791 the lower-hybrid drift instability," *Phys. Rev. Lett.* **123**, 235101 (2019).
792 ³⁵J. L. Burch, R. B. Torbert, T. D. Phan, L.-J. Chen, T. E. Moore, R. D. Ergun, J.
793 P. Eastwood, D. J. Gershman, P. A. Cassak, M. R. Argall, S. Wang, M. Hesse, C.
794 J. Pollock, B. L. Giles, R. Nakamura, B. H. Mauk, S. A. Fuselier, C. T. Russell, R.
795 J. Strangeway, J. F. Drake, M. A. Shay, Y. V. Khotyaintsev, G. Lindqvist, P.-A.
796 Marklund, F. D. Wilder, D. T. Young, K. Torkar, J. Goldstein, J. C. Dorelli, L.
797 A. Avanov, M. Oka, D. N. Baker, A. N. Jaynes, K. A. Goodrich, I. J. Cohen, D.
798 L. Turner, J. F. Fennell, J. B. Blake, J. Clemmons, M. Goldman, D. Newman, S.
799 M. Petrinec, K. J. Trattner, B. Lavraud, P. H. Reiff, W. Baumjohann, W.
800 Magnes, M. Steller, W. Lewis, Y. Saito, V. Coffey, and M. Chandler, "Electron-
801 scale measurements of magnetic reconnection in space," *Science* **352**, 1176
802 (2016).
803 ³⁶R. B. Torbert, C. T. Russell, W. Magnes, R. E. Ergun, P.-A. Lindqvist, O.
804 LeContel, H. Vaith, J. Macri, S. Myers, D. Rau, J. Needell, B. King, M. Granoff,
805 M. Chutter, I. Dors, G. Olsson, Y. V. Khotyaintsev, A. Eriksson, C. A. Kletzing,
806 S. Bounds, B. Anderson, W. Baumjohann, M. Steller, K. Bromund, G. Le, R.
807 Nakamura, R. J. Strangeway, H. K. Leinweber, S. Tucker, J. Westfall, D.
808 Fischer, F. Plaschke, J. Porter, and K. Lappalainen, "The *FIELDS* instrument
809 suite on *MMS*: Scientific objectives, measurements, and data products," *Space
810 Sci. Rev.* **199**, 105–135 (2016).
811 ³⁷C. T. Russell, B. J. Anderson, W. Baumjohann, K. R. Bromund, D. Dearborn,
812 D. Fischer, G. Le, H. K. Leinweber, D. Leneman, W. Magnes, J. D. Means, M.
813 B. Moldwin, R. Nakamura, D. Pierce, F. Plaschke, K. M. Rowe, J. A. Slavin, R. J.
814 Strangeway, R. Torbert, C. Hagen, I. Jernej, A. Valavanoglou, and I. Richter,
815 "The Magnetospheric Multiscale Magnetometers," *Space Sci. Rev.* **199**,
816 189–256 (2016).
817 ³⁸R. E. Ergun, S. Tucker, J. Westfall, K. A. Goodrich, D. M. Malaspina, D.
818 Summers, J. Wallace, M. Karlsson, J. Mack, N. Brennan, B. Pyke, P. Withnell,
819 R. Torbert, J. Macri, D. Rau, I. Dors, J. Needell, P.-A. Lindqvist, G. Olsson, and
820 C. M. Cully, "The axial double probe and fields signal processing for the *MMS*
821 mission," *Space Sci. Rev.* **199**, 167–188 (2016).
822 ³⁹P.-A. Lindqvist, G. Olsson, R. B. Torbert, B. King, M. Granoff, D. Rau, G.
823 Needell, S. Turco, I. Dors, P. Beckman, J. Macri, C. Frost, J. Salwen, A.
824 Eriksson, L. Åhlén, Y. V. Khotyaintsev, J. Porter, K. Lappalainen, R. E. Ergun,
825 W. Wermeier, and S. Tucker, "The spin-plane double probe electric field instru-
826 ment for *MMS*," *Space Sci. Rev.* **199**, 137–165 (2016).
⁴⁰C. Pollock, T. Moore, A. Jacques, J. Burch, U. Gliese, Y. Saito, T. Omoto, L. 827
Avanov, A. Barrie, V. Coffey, J. Dorelli, D. Gershman, B. Giles, T. Rosnack, C. 828
Salo, S. Yokota, M. Adrian, C. Aoustin, C. Auletta, S. Aung, V. Bigio, N. Cao, 829
M. Chandler, D. Chornay, K. Christian, G. Clark, G. Collinson, T. Corris, A. 830
De Los Santos, R. Devlin, T. Diaz, T. Dickerson, C. Dickson, A. Diekmann, F. 831
Diggs, C. Duncan, A. Figueroa-Vinas, C. Firman, M. Freeman, N. Galassi, K. 832
García, G. Goodhart, D. Guerrerro, J. Hageman, J. Hanley, E. Hemminger, M. 833
Holland, M. Hutchins, T. James, W. Jones, S. Kreisler, J. Kujawski, V. Lavu, J. 834
Lobell, E. LeCompte, A. Lukemire, E. MacDonald, A. Mariano, T. Mukai, K. 835
Narayanan, Q. Nguyen, M. Onizuka, W. Paterson, S. Persyn, B. Piepgrass, F. 836
Cheney, A. Rager, T. Raghuram, A. Ramil, L. Reichenthal, H. Rodriguez, J. 837
Rouzaud, A. Rucker, Y. Saito, M. Samara, J.-A. Sauvaud, D. Schuster, M. 838
Shappirio, K. Shelton, D. Sher, D. Smith, K. Smith, S. Smith, D. Steinfeld, R. 839
Szymkiewicz, K. Tanimoto, J. Taylor, C. Tucker, K. Tull, A. Uhl, J. Vloet, P. 840
Walpole, S. Weidner, D. White, G. Winkert, P.-S. Yeh, and M. Zeuch, "Fast 841
Plasma Investigation for Magnetospheric Multiscale," *Space Sci. Rev.* **199**,
331–406 (2016). 842
⁴¹D. J. Gershman, J. C. Dorelli, A. F.-Viñas, and C. J. Pollock, "The calculation of 843
moment uncertainties from velocity distribution functions with random 844
errors," *J. Geophys. Res.: Space Phys.* **120**, 6633–6645, [https://doi.org/10.1002/
845 2014JA020775](https://doi.org/10.1002/2014JA020775) (2015). 846
⁴²D. T. Young, J. L. Burch, R. G. Gomez, A. De Los Santos, G. P. Miller, P. 847
Wilson, N. Paschalidis, S. A. Fuselier, K. Pickens, E. Hertzberg, C. J. Pollock, J. 848
Scherrer, P. B. Wood, E. T. Donald, D. Aaron, J. Furman, D. George, R. S. 849
Gurnee, R. S. Hourani, A. Jacques, T. Johnson, T. Orr, K. S. Pan, S. Persyn, S. 850
Pope, J. Roberts, M. R. Stokes, K. J. Trattner, and J. M. Webster, "Hot plasma 851
composition analyzer for the Magnetospheric Multiscale Mission," *Space Sci.* 852
Rev. **199**, 407–470 (2016). 853
⁴³G. Chanteur and C. Harvey, "Spatial interpolation for four spacecraft: 854
Application to magnetic gradients," in *Analysis Methods for Multi-Spacecraft* 855
Data, ISSI Scientific Report SR-001, edited by G. Paschman and P. Daly 856
(European Space Agency, 1998), Chap. 15, pp. 371–393. 857
⁴⁴B. U. Ö. Sonnerup and M. Scheible, "Minimum and maximum variance analy- 858
sis," in *ISSI Scientific Reports Series* (■, 1998), Vol. 1, pp. 185–220. 859
⁴⁵H. S. Fu, Y. V. Khotyaintsev, A. Vaivads, M. André, V. A. Sergeev, S. Y. Huang, 860
E. A. Kronberg, and P. W. Daly, "Pitch angle distribution of suprathermal elec- 861
trons behind dipolarization fronts: A statistical overview," *J. Geophys. Res.:* 862
Space Phys. **117**, A12221 (2012). 863
⁴⁶Z. Yao, W. J. Sun, S. Y. Fu, Z. Y. Pu, J. Liu, V. Angelopoulos, X. J. Zhang, X. N. 864
Chu, Q. Q. Shi, R. L. Guo, and Q. G. Zong, "Current structures associated with 865
dipolarization fronts," *J. Geophys. Res.: Space Phys.* **118**, 6980–6985, [https://
866 doi.org/10.1002/2013JA019290](https://doi.org/10.1002/2013JA019290) (2013). 867
⁴⁷H. S. Fu, Y. V. Khotyaintsev, M. André, and A. Vaivads, "Fermi and betatron 868
acceleration of suprathermal electrons behind dipolarization fronts," *Geophys.* 869
Res. Lett. **38**, L16104, <https://doi.org/10.1029/2011GL048528> (2011). 870
⁴⁸A. T. Y. Lui, Y. Zheng, H. Rème, M. W. Dunlop, G. Gustafsson, and C. J. 871
Owen, "Breakdown of the frozen-in condition in the Earth's magnetotail," 872
J. Geophys. Res.: Space Phys. **112**, A04215 (2007). 873
⁴⁹R. B. Torbert, J. L. Burch, B. L. Giles, D. Gershman, C. J. Pollock, J. Dorelli, L. 874
Avanov, M. R. Argall, J. Shuster, R. J. Strangeway, C. T. Russell, R. E. Ergun, F. 875
D. Wilder, K. Goodrich, H. A. Faith, C. J. Farrugia, P. A. Lindqvist, T. Phan, Y. 876
Khotyaintsev, T. E. Moore, G. Marklund, W. Daughton, W. Magnes, C. A. 877
Kletzing, and S. Bounds, "Estimates of terms in Ohm's law during an encoun- 878
ter with an electron diffusion region," *Geophys. Res. Lett.* **43**, 5918–5925, 879
<https://doi.org/10.1002/2016GL069553> (2016). 880
⁵⁰J. Birn and M. Hesse, "Energy release and conversion by reconnection in the 881
magnetotail," *Ann. Geophys.* **23**, 3365–3373 (2005). 882
⁵¹Y. Xu, H. Fu, J. Cao, C. Liu, C. Norgren, and Z. Chen, "Electron scale measure- 883
ments of antidipolarization front," *Geophys. Res. Lett.* **48**, e92232, [https://
884 doi.org/10.1029/2020GL092232](https://doi.org/10.1029/2020GL092232) (2021). 885
⁵²J. E. Stawarz, J. P. Eastwood, K. J. Genestreti, R. Nakamura, R. E. Ergun, D. 886
Burgess, J. L. Burch, S. A. Fuselier, D. J. Gershman, B. L. Giles, O. Le Contel, P. 887
A. Lindqvist, C. T. Russell, and R. B. Torbert, "Intense electric fields and 888
electron-scale substructure within magnetotail flux ropes as revealed by the 889
Magnetospheric Multiscale Mission," *Geophys. Res. Lett.* **45**, 8783–8792, 890
<https://doi.org/10.1029/2018GL079095> (2018). 891
892

- 893 ⁵³R. C. Davidson and N. T. Gladd, “Anomalous transport properties associated
894 with the lower-hybrid-drift instability,” *Phys. Fluids* **18**, 1327–1335 (1975).
- 895 ⁵⁴J. D. Huba, N. T. Gladd, and K. Papadopoulos, “Lower-hybrid-drift wave tur-
896 bulence in the distant magnetotail,” *J. Geophys. Res.: Space Phys.* **83**,
897 5217–5226, <https://doi.org/10.1029/JA083iA11p05217> (1978).
- 898 ⁵⁵L. J. Chen, S. Wang, O. Le Contel, A. Rager, M. Hesse, J. Drake, J. Dorelli, J.
899 Ng, N. Bessho, D. Graham, L. B. Wilson, T. Moore, B. Giles, W. Paterson, B.
900 Lavraud, K. Genestreti, R. Nakamura, Y. V. Khotyaintsev, R. E. Ergun, R. B.
901 Torbert, J. Burch, C. Pollock, C. T. Russell, P. A. Lindqvist, and L. Avakov,
902 “Lower-hybrid drift waves driving electron nongyrotropic heating and vortical
903 flows in a magnetic reconnection layer,” **125**, 025103 (2020).
- 904 ⁵⁶V. Angelopoulos, P. Cruce, A. Drozdov, E. W. Grimes, N. Hatzigeorgiu, D. A.
905 King, D. Larson, J. W. Lewis, J. M. McTiernan, D. A. Roberts, C. L. Russell, T.
906 Hori, Y. Kasahara, A. Kumamoto, A. Matsuoka, Y. Miyashita, Y. Miyoshi, I.
907 Shinohara, M. Teramoto, J. B. Faden, A. J. Halford, M. McCarthy, R. M.
908 Millan, J. G. Sample, D. M. Smith, L. A. Woodger, A. Masson, A. A. Narock, K.
909 Asamura, T. F. Chang, C. Y. Chiang, Y. Kazama, K. Keika, S. Matsuda, T.
910 Segawa, K. Seki, M. Shoji, S. W. Y. Tam, N. Umemura, B. J. Wang, S. Y. Wang,
R. Redmon, J. V. Rodriguez, H. J. Singer, J. Vandegriff, S. Abe, M. Nose, A. Shinbori, Y. M. Tanaka, S. UeNo, L. Andersson, P. Dunn, C. Fowler, J. S. Halekas, T. Hara, Y. Harada, C. O. Lee, R. Lillis, D. L. Mitchell, M. R. Argall, K. Bromund, J. L. Burch, I. J. Cohen, M. Galloy, B. Giles, A. N. Jaynes, O. Le Contel, M. Oka, T. D. Phan, B. M. Walsh, J. Westlake, F. D. Wilder, S. D. Bale, R. Livi, M. Pulupa, P. Whittlesey, A. DeWolfe, B. Harter, E. Lucas, U. Auster, J. W. Bonnell, C. M. Cully, E. Donovan, R. E. Ergun, H. U. Frey, B. Jackel, A. Keiling, H. Korth, J. P. McFadden, Y. Nishimura, F. Plaschke, P. Robert, D. L. Turner, J. M. Weygand, R. M. Candey, R. C. Johnson, T. Kovalick, M. H. Liu, R. E. McGuire, A. Breneman, K. Kersten, and P. Schroeder, “The space physics environment data analysis system (SPEDAS),” *Space Sci. Rev.* **215**, 9 (2019).
- ⁵⁷J. Burch, *Magnetospheric Multiscale Mission* (Laboratory for Atmospheric and Space Physics (LASP) at the University of Colorado, Boulder, 2015).
- ⁵⁸R. C. Davidson, N. T. Gladd, C. S. Wu, and J. D. Huba, “Effects of finite plasma beta on the lower-hybrid-drift instability,” *Phys. Fluids* **20**, 301–310 (1977).
- ⁵⁹C. Norgren, A. Vaivads, Y. V. Khotyaintsev, and M. André, “Lower hybrid drift waves: Space observations,” *Phys. Rev. Lett.* **109**, 055001 (2012).

AQ9